

## Manuscript Details

<b>Manuscript number</b>	PROOCE_2017_188_R1
<b>Title</b>	Bottom trawling at Whittard Canyon: evidence for seabed modification, trawl plumes and food source heterogeneity
<b>Article type</b>	Full Length Article

### Abstract

Fishing vessels are attracted to the dendritic Whittard Canyon system due to the abundance and diversity of species found there. Both midwater and bottom trawling are commonplace, including on deep canyon channel floors. Bottom trawling is identified here as a possible cause of changes to seafloor roughness along the canyon interfluves. An Arc Chord Ratio (ACR) rugosity index is calculated for the Whittard area and correlated with Vessel Monitoring System (VMS) data using various statistical models. Over higher slopes or rougher ground the heavily fished locations show a more homogeneous rugosity distribution than those lightly fished, indicating possible smoothing of the seabed. Bottom trawling activity on adjacent interfluves/shelf is known to generate energetic turbid, sediment plumes within the canyon branches to 2500 m depth, with elevated Suspended Particulate Matter (SPM) concentrations in the water column up to 400 m above the seabed. Lipid biomarker analysis of organic material collected from these plumes showed higher concentrations of total lipids at sites that are intensively trawled (east). In comparison to sites that are less intensively trawled (west), higher contributions of fatty alcohols were detected. While lower concentrations of unsaturated fatty acids were detected, biomarkers indicative of phytoplankton accounted for  $93.4 \pm 0.7\%$  of total lipids identified from eastern samples suggesting rapid transport of labile compounds. Results presented here suggest that intensive trawling induced changes to sediment transport will complicate the interpretation of biogeochemical property distributions at canyon systems, particularly from single surveys. Anthropogenically generated heterogeneity in sediment supply and character will also impact on habitat suitability for resident ecosystems.

<b>Keywords</b>	Trawling Plumes; Whittard Canyon; Suspended Particulate Matter; Vessel Monitoring System; Rugosity Index; Lipid Biomarkers
<b>Manuscript category</b>	Interdisciplinary
<b>Corresponding Author</b>	Eoghan Daly
<b>Corresponding Author's Institution</b>	National University of Ireland, Galway
<b>Order of Authors</b>	Eoghan Daly, Mark Johnson, Annette Wilson, Hans Gerritsen, Kostas Kiriakoulakis, Louise Allcock, martin white
<b>Suggested reviewers</b>	Alexis Khripounoff, Serge Heussner, Albert Palanques

## Submission Files Included in this PDF

### File Name [File Type]

Trawling\_Whittard\_INCISE\_Responses\_301117.docx [Response to Reviewers]

Highlights\_301117.docx [Highlights]

Trawling\_Whittard\_INCISE\_REVISION\_291117.docx [Manuscript File]

Trawling\_Whittard\_INCISE\_Figures\_and\_Tables\_301117.docx [Figure]

To view all the submission files, including those not included in the PDF, click on the manuscript title on your EVISE Homepage, then click 'Download zip file'.

## **Bottom trawling at Whittard Canyon: evidence for seabed modification, trawl plumes and food source heterogeneity, Daly et al., Ref: PROOCE\_2017\_188**

We are grateful for the opportunity of submitting a revised version of our manuscript for the upcoming INCISE special edition. We would like to thank the reviewers for their constructive comments and suggestions which have significantly improved the revised manuscript. In response to the major and minor review comments, we have re-written and re-structured substantial parts of the manuscript as indicated below, but with particular reference to improving figure quality, combining the different methods and drawing some more substantial conclusions to the analysis. We have addressed all comments and suggestions and we note that both reviewers have expressed concerns about the crossover between this work and that of Wilson et al., (2015a, b). This was an error in over referencing the previous work to set the new results in context, which has now been revised.

Specific responses to individual reviewers are summarised below.

### **Reviewer 1**

We have slightly amended the title of the manuscript to add reference to each aspect of the work and hopefully retain or increase its impact. The discussion section has undergone considerable re-working based on the suggestions given.

#### **Comments:**

Line 61: Reviewer 2's suggested citation was incorporated here.

Line 69: This has been clarified by making distinction between trawl doors and other ground gear.

Line 84: Changed to: adjacent to, and within

Line 85: Now described as natural 'transport' processes, we would consider that transport via riverine input could be seen as a process in the context of a canyon system.

Lines 480 onwards: The point about fishing grounds in close proximity to very steep slopes has been added (line 519) as has the fact that not all resuspended material will be transported (line 525).

Lines 496-497: In the interest of clarity the word ‘novel’ has been dropped.

Lines 507-510: New datasets are, as yet, unprocessed and a research output is many months (or years) from completion.

Line 529 onwards: The discussion of the trawling plumes has been re-written, and in that section and throughout discussion, the importance of trawl plumes has had its emphasis increased. The intention of the comparison of the turbulent dissipation estimates (not current speeds) with non-trawl plumes was more to show that the values deduced from the basic analysis were not inappropriate for a gravity flow. The section has been re-written to take this into account.

In general, the discussion section has been rewritten to provide a more coherent and stronger set of comparisons, implications and conclusions.

### **Figures:**

Fig 2: To reduce confusion this figure has been split in two with part (a) introducing the region’s bathymetry and areas of interest and includes depth contours. Part (b) introduces fishing effort. Many colour schemes were sampled but the original was preferred.

Fig 3: Thank you for pointing out the flaws of this figure. It has been removed and replaced. The new figure 3 shows maps of slope and rugosity for the region. It was not possible to display a VMS fishing grid overlaying slope or rugosity without confusion or colours clashing. Instead, contours of VMS fishing have been added to rugosity. Depth contours were retained with the slope map for further information.

Fig 5 (previously Fig 4): This figure stems from an initial analysis of the data and depicts the variation in rugosity (rather than rugosity itself) as it changes with increasing slope. This can be seen as a proxy for ‘heterogeneity’ of seafloor roughness. Description of this has been strengthened in the text (line 334).

Fig 7 (previously Fig 6): We appreciate that the presentation of two along channel sections could be skewed by the aliasing of the data (mostly in the near seabed data) so a new approach was used. Here the post trawling event is still shown as the intention was to highlight that the channel is filled to several 100 metres above bottom with significantly enhanced SPM concentrations. We have also included where maximum SPM concentrations

were found under natural conditions (as discussed by Wilson et al 2015) as a comparison for perspective. We have followed the suggestion to show (here selected) profiles as well to highlight the near seabed changes.

Fig 11 (previously Fig 10): While discussing benthic lifeforms and food source heterogeneity this figure is designed to aid the reader (especially non-experts) in visualising the sedimentary conditions experienced. This figure is not claimed as a result of analysis and the text (and caption) has been improved to reflect this. We would like to retain this figure.

## **Reviewer 2**

With respect to the writing style, edits have been made to make the text more concise.

References have been added as per PDF comments.

Restructuring has taken place between sections as per PDF comments. These and further restructuring of the introduction and discussion sections provides a more defined framework to the manuscript.

With the helpful comments of both reviewers, we now realise how it could appear like we are presenting previous work carried out by Wilson et al., (2015a) again here. We have endeavoured to highlight the development of the new work/results from the old throughout the revised manuscript.

With respect to VMS data, there is a misconception that the data is a census of fishing activity rather than a statistical representation. This has now been described in detail including statistical errors in the methods section. As far as I am aware AIS data is currently only available closer to shore, within VHF radio range (10-20 nautical miles), although newer satellite systems (SAIS) are presently coming on-stream.

An appendix of GAMs mathematics has not been included, because it is incredibly difficult to glean the precise mathematics used by the models. This is due to the fact that the internal mathematics seem to be only accessible through computer code in R. Instead there is a general GAMs model equation and description added to the methods section which includes references to literature and code for any reader wishing to pursue it further.

Following are replies to specific numbered PDF comments. Any comments dealt with above or changed exactly as recommended are not included below.

**Comments:**

[Comments 2-4]: Text has been re-written

[Comment 10]: A sentence has not been added here about detailed calculations of global trawled area. It has been mentioned briefly in sentence one of this paragraph. At time of writing, the book Submarine Geomorphology was not available, nor do we currently have access to it, therefore we plan not to use it.

[Comment 12]: This sentence has been changed in line with suggestions from Reviewer 1

[Comment 13]: Halpern et al., (2008) has been included but Oberle et al., (2018) has not, as mentioned above

[Comments 14, 15]: Wilson et al., (2015a) did not analyse sediment dynamics (lines 125-127). Further clarifications are to follow in the writing e.g. biogeochemical analysis here is new additional analysis on the samples described in Wilson et al., (2015a)

[Comments 16-18]: Please see new writing addressing in detail the concerns over VMS data, how it was filtered and inclusion of errors

[Comment 19]: Wilson et al., (2015a) has been removed here. They essentially just named the canyon branches as WC1-4 and this work simply carries on using the same naming convention. GIS analysis carried out for this paper occurred after Wilson et al., (2015a) was published

[Comment 22]: Please note these errors quoted are for 'fishing effort (hrs)' (line 323) and are different to the errors mentioned for 'fishing records' (lines 167-169)

[Comment 23]: This has been added as part of Fig. 6 (previously Fig. 5)

[Comments 24, 25]: This paragraph has been re-written to be more descriptive and explanatory of the results of Fig 6 (previously Fig 5), however, in the interest of aesthetics, graphics were not added to the figure to point out the deflecting contours above 10 degrees.

[Comment 26]: This new figure has been added as Fig. 4 and placed before the old Fig. 4 because it came earlier in the analysis process.

[Comment 30]: lines 381-384 address the difference between Wilson et al., (2015a) and this work.

[Comments 32-34]: This section has been re-written in line with the new figure

[Comments 39-41]: This text has been moved to methods section

[Comments 42, 43]: Revised

[Comment 44]: We agree that the word typical was used too much and has been edited where appropriate. It was a reference to conditions under the natural (i.e. non-plume) driving forces that have been identified previously. That is now stated in the text.

[Comment 50]: We are unsure how to present the results of our statistical analysis as percentages.

[Comment 55]: We do not have any data for sediment sizes within Whittard and published data are referenced elsewhere in the text (Amaro et al., 2016). We have, however, re-written the sentence in question to improve on its detail.

[Comment 56]: This has been rephrased.

[Comment 57]: It is unclear as to the specifics of this comment. An effort has been made to improve the text in connection to this figure.

[Comment 61]: Text has been enhanced in this paragraph and the figure caption has been amended. Please also see response comments to reviewer 1 above, on this matter (Fig 11).

## **Highlights**

- Evidence for seabed modification by bottom trawling activity
- Trawl plume material and associated energy dissipates down canyon channels
- Heterogeneity in down canyon organic transport varies with trawling variability
- Heterogeneity may cause complication in interpreting biogeochemical distribution

1  
2  
3  
4 1 **Bottom trawling at Whittard Canyon: evidence for seabed**  
5 2 **modification, trawl plumes and food source heterogeneity**  
6  
7 3

8  
9 4 Eoghan Daly<sup>1,2</sup>, Mark P. Johnson<sup>1</sup>, Annette M. Wilson<sup>3</sup>, Hans D. Gerritsen<sup>4</sup>, Konstadinos  
10 5 Kiriakoulakis<sup>5</sup>, A. Louise Allcock<sup>6</sup> and Martin White<sup>1,2</sup>.  
11 6

- 12  
13 7 1. Earth and Ocean Sciences, Ryan Institute - School of Natural Sciences, National  
14 8 University of Ireland, Galway, Ireland.  
15 9 2. Irish Centre for Research in Applied Geoscience (ICRAG), National University of Ireland,  
16 10 Galway, Ireland.  
17 11 3. Alfred Wegener Institute, Biologische Anstalt Helgoland, 27498 Helgoland, Germany.  
18 12 4. Marine Institute, Rinville, Oranmore, Co. Galway, Ireland.  
19 13 5. Natural Sciences and Psychology, Liverpool John Moores University, UK.  
20 14 6. Zoology, Ryan Institute - School of Natural Sciences, National University of Ireland,  
21 15 Galway, Ireland.  
22 16  
23 17

24  
25  
26 18 **Abstract**  
27

28  
29 19 Fishing vessels are attracted to the dendritic Whittard Canyon system due to the abundance  
30 20 and diversity of species found there. Both midwater and bottom trawling are commonplace,  
31 21 including on deep canyon channel floors. Bottom trawling is identified here as a possible  
32 22 cause of changes to seafloor roughness along the canyon interfluves. An Arc Chord Ratio  
33 23 (ACR) rugosity index is calculated for the Whittard area and correlated with Vessel  
34 24 Monitoring System (VMS) data using various statistical models. Over higher slopes or  
35 25 rougher ground the heavily fished locations show a more homogeneous rugosity distribution  
36 26 than those lightly fished, indicating possible smoothing of the seabed.  
37

38  
39 27 Bottom trawling activity on adjacent interfluves/shelf is known to generate energetic turbid,  
40 28 sediment plumes within the canyon branches to 2500 m depth, with elevated Suspended  
41 29 Particulate Matter (SPM) concentrations in the water column up to 400 m above the seabed.  
42 30 Lipid biomarker analysis of organic material collected from these plumes showed higher  
43 31 concentrations of total lipids at sites that are intensively trawled (east). In comparison to sites  
44 32 that are less intensively trawled (west), higher contributions of fatty alcohols were detected.  
45 33 While lower concentrations of unsaturated fatty acids were detected, biomarkers indicative of  
46 34 phytoplankton accounted for 93.4±0.7% of total lipids identified from eastern samples  
47 35 suggesting rapid transport of labile compounds. Results presented here suggest that intensive  
48  
49  
50  
51  
52  
53  
54  
55  
56  
57  
58  
59

60  
61  
62 36 trawling induced changes to sediment transport will complicate the interpretation of  
63  
64 37 biogeochemical property distributions at canyon systems, particularly from single surveys.  
65  
66 38 Anthropogenically generated heterogeneity in sediment supply and character will also impact  
67  
68 39 on habitat suitability for resident ecosystems.  
69  
70 40

71  
72 41 **Keywords:** Trawling Plumes; Whittard Canyon; Suspended Particulate Matter; Vessel  
73  
74 42 Monitoring System; Rugosity Index; Lipid Biomarkers  
75  
76 43

## 77 44

## 78 45 **1. Introduction**

## 79 46

80  
81  
82  
83  
84  
85  
86 47 The continental margin, occupying a little over 10% of the ocean surface area, connects the  
87  
88 48 shelf seas (and hence coastal regions) to the deep sea, plays a significant role in the provision  
89  
90 49 of food and energy resources, is a site for biogeochemical cycling (including carbon  
91  
92 50 sequestration), and hosts a range of diverse ecosystem habitats and associated ecosystem  
93  
94 51 services (e.g. [Levin and Dayton, 2009](#); [Benn et al., 2010](#); [Levin and Sibuet, 2012](#)). The  
95  
96 52 margin is an area of heterogeneous habitat driven, in part, by the variation in continental  
97  
98 53 morphology and topographic features, including slope variations, banks, mounds, seeps and  
99  
100 54 canyons ([Levin et al., 2010](#)). In particular, sedimentary slopes are the most extensive margin  
101  
102 55 habitat and contain the most numerous and diverse benthic communities ([Grassle and](#)  
103  
104 56 [Maciolek, 1997](#); [Levin and Sibuet, 2012](#)). There is a growing anthropogenic impact at these  
105  
106 57 margin environments (e.g. [Eastwood et al., 2007](#); [Benn et al., 2010](#); [Doney, 2010](#); [Ramirez-](#)  
107  
108 58 [Llodra et al., 2011](#)). In particular, the spatial expansion of bottom trawling ([Morato et al.,](#)  
109  
110 59 [2006](#)) into the deeper environment has been recognized as a significant element in modifying  
111  
112 60 both seabed morphology and the sediment flux across the margin (e.g. [Benn et al., 2010](#); [Puig](#)  
113  
114 61 [et al., 2012](#); [Martín et al., 2014b](#); [Oberle et al., 2016a](#)). Both anthropogenic and natural  
115  
116 62 drivers of ecosystem change at the continental margin require further quantification as a  
117  
118 63 foundation for offshore resource management and conservation (e.g. [Davies et al., 2007](#);  
64 [Benn et al., 2010](#)).

119  
120  
121 65 Bottom trawling covers ground area comparable to between half (Watling and Norse, 1998)  
122 66 and three quarters (Kaiser et al., 2002) of the world's continental shelves, can globally drive  
123 67 sediment flux similar in quantity to fluvial input (Oberle et al., 2016a) and can have greater  
124 68 impact on the seabed than all other anthropogenic pressures combined (Eastwood et al., 2007;  
125 69 Halpern et al., 2008; Benn et al., 2010). These impacts are exacerbated in deeper, off-shelf  
126 70 waters where background energy levels and species resilience is lower and habitat recovery  
127 71 time slower (Kaiser et al., 2002). Bottom trawling gear makes direct contact with the seafloor  
128 72 and is responsible for the sorting and layering of sediments, for overturning, breaking up  
129 73 sediment fabric and causing bed armouring (Martín et al., 2014a; Oberle et al., 2016b). The  
130 74 degree to which the seafloor is affected depends on bottom type, gear design and ground  
131 75 contact (Gerritsen et al., 2013), with trawl doors causing the most acute damage (O'Neill and  
132 76 Summerbell, 2011), while sweep lines, bridals and footropes cause the most widespread  
133 77 damage (Martín et al., 2014b). In addition to physical alterations, trawling activity can also  
134 78 alter the biogeochemical composition of local sediments (Pusceddu et al., 2005a, b), with  
135 79 compositional changes being more influential than the seasonal input of organic matter in  
136 80 some areas (Sañe et al., 2013). Fishing grounds commonly have lower concentrations of  
137 81 flocculent Organic Carbon (OC) due to winnowing and oxygenation (Martín et al., 2014a;  
138 82 Pusceddu et al., 2014). Given these significant changes, the resuspension of organic matter  
139 83 from coastal and shelf regions by bottom trawling will likely increase OC export rates to the  
140 84 deep (Martín et al., 2008; Palanques et al., 2014). Furthermore, heavy metals and other  
141 85 pollutants buried in coastal sediments can be released by trawling activity and transported to  
142 86 deeper more vulnerable areas (Jones, 1992; Palanques et al., 1994).

143  
144  
145  
146  
147  
148  
149  
150  
151  
152  
153  
154  
155  
156  
157 87 Submarine canyons provide a conduit for sediment flux between the shelf and deep ocean  
158 88 along the world's continental margins and, as such, both the deep sea and submarine canyons  
159 89 are now recognised as potential major repositories for anthropogenic wastes and marine litter,  
160 90 including plastics (e.g. Pham et al., 2014). There are many natural transport processes that  
161 91 control sediment erosion, transportation and deposition adjacent to, and within, submarine  
162 92 canyons, such as storm waves (Sanchez-Vidal et al., 2012), river input (Khrifounoff et al.,  
163 93 2009), dense shelf water cascading (Canals et al., 2006) and slope failure, each dependent on  
164 94 local or regional physical conditions. When compared to natural canyon transport processes  
165 95 that drive sediment flux, several studies have discussed anthropogenic impact, through  
166 96 bottom trawling, as a major, if not dominant, process, especially on human time scales (e.g.  
167 97 Halpern et al., 2008; Puig et al., 2012; Martín et al., 2014b; Puig et al., 2014). Additionally,  
168  
169  
170  
171  
172  
173  
174  
175  
176  
177

178  
179  
180 98 bottom trawling in proximity to submarine canyons has been found to smooth out the  
181  
182 99 seascape on large spatial scales, for example, at La Fonera Canyon (Puig et al., 2012; Martín  
183 et al., 2014a; Martín et al., 2014c; Payo-Payo et al., 2017), where changes to topography are  
184 100  
185 101 now clearly visible on high resolution bathymetry maps (Puig et al., 2012). Trawler induced  
186  
187 102 sediment gravity flows in La Fonera Canyon have been described in detail by Martín et al.  
188  
189 103 (2014c). Payo-Payo et al. (2017) highlighted, through modelling anthropogenic sediment  
190 104 resuspension/transport, the ability of bottom trawling to affect wider areas than the fishing  
191  
192 105 grounds, contrasting localised resettling on-shelf and over canyon flanks with widespread and  
193 106 distal displacement from sediment turbidity currents, especially over the steeper slopes.

195  
196 107 Changes to morphology and biogeochemistry caused by bottom trawling in submarine  
197 108 canyons can affect ecosystem functioning and massively reduce benthic habitat heterogeneity  
198  
199 109 (Watling and Norse, 1998; Puig et al., 2012 and references within). Trawling of the seafloor,  
200 110 negatively impacts on the biodiversity and abundance of life found there (Watling and Norse,  
201  
202 111 1998; Puig et al., 2012; Pusceddu et al., 2014); greatly reducing infaunal communities  
203  
204 112 (O'Neill and Summerbell, 2011) when compared to untrawled areas.

205  
206 113 In this paper the potential impacts of fishing on seabed morphology and down-canyon  
207 114 sediment distribution and associated biogeochemical parameters at the Whittard Canyon  
208  
209 115 system on the Celtic Sea margin, NE Atlantic (Fig.1) have been assessed. The Whittard  
210  
211 116 Canyon is a dendritic system with canyon heads cutting the shelf at 180–200 m and a main  
212  
213 117 channel axis opening onto deep ocean floor at 3600–4400 m (Reid and Hamilton, 1990;  
214 118 Amaro et al., 2016). Whittard Canyon has limited sediment input from fluvial processes due  
215  
216 119 to its distance (~ 300 km) from land, but does experience significant off-shelf material flux.  
217  
218 120 This is due to high overlying pelagic productivity (Sharples et al., 2013) and dynamical  
219 121 processes such as boundary currents and internal waves which drive transport via nepheloid  
220  
221 122 layers (Wilson 2015b; Hall et al., 2017), slope failure and sediment gravity flows (Amaro et  
222 123 al., 2016). Additionally, Wilson et al. (2015a) observed Enhanced bottom Nepheloid Layers  
223  
224 124 (ENLs) with significantly higher sediment concentrations in two branches of Whittard  
225  
226 125 Canyon. These ENLs were correlated with fishing activity, via Vessel Monitoring System  
227 126 (VMS) data, to determine their anthropogenic origin but no detailed analysis of the plume  
228  
229 127 dynamics were made at that time.

230  
231 128 [Figure 1 here please, at 1.5 columns wide]  
232  
233  
234  
235  
236

237  
238  
239  
240  
241  
242  
243  
244  
245  
246  
247  
248  
249  
250  
251  
252  
253  
254  
255  
256  
257  
258  
259  
260  
261  
262  
263  
264  
265  
266  
267  
268  
269  
270  
271  
272  
273  
274  
275  
276  
277  
278  
279  
280  
281  
282  
283  
284  
285  
286  
287  
288  
289  
290  
291  
292  
293  
294  
295

129 Results are presented here in two parts; (i) a statistical comparison of fishing intensity and  
130 seafloor rugosity is carried out through a generalized additive model (GAM) fit, and (ii) a  
131 brief assessment is made of the dynamical and biogeochemical characteristics of the resulting  
132 trawl-induced sediment plumes found in the Whittard Canyon branches. Results are discussed  
133 with respect to potential issues in interpretation of suspended sediment distribution patterns,  
134 biogeochemical signatures and potential impacts on ecosystem functioning within this and  
135 similar canyon systems.

136

## 137 **2. Methods**

138

### 139 *2.1. Spatially distributed fishing intensity and seafloor roughness*

140 Vessel Monitoring Systems (VMS) are used internationally for tracking vessel activity  
141 including fishing vessels. In the Whittard region, the fishing activity consists of northern and  
142 southern European fishing fleets. The spatial distribution of fishing fleets can change due to  
143 factors such as targeting different specific species or the cost of fuel (Gerritsen and Lordan,  
144 2011). VMS monitoring is administered within the Irish Exclusive Economic Zone (EEZ) by  
145 the Irish Naval Service. Speed and position data are sent via satellite from each vessel at a  
146 minimum frequency of once every two hours. VMS data for this study were extracted for the  
147 period from January 2006 to February 2016 and then linked to logbook data to identify the  
148 gear type used (following methods described by Gerritsen and Lordan, 2011). Only bottom  
149 trawling vessels (which directly affect the seafloor) were retained in the dataset. Gear types  
150 used were bottom otter trawls (OTB), bottom pair trawls (PTB) and otter twin trawls (OTT)  
151 (Nédélec and Prado, 1990). Fishing effort was defined according to Gerritsen and Lordan  
152 (2011). Each VMS record was assigned an effort value that was equal to the time interval  
153 since the previous record (generally 2 h). Records with time intervals > 4 h were given an  
154 effort value of 4 h. The data were then filtered to exclude vessel speeds < 0.5 knots or > 4.5  
155 knots in order to retain only the records that correspond to fishing activity. VMS data were  
156 then gridded to their provided resolution of 0.01 x 0.01 decimal degrees, or 740 m (east/west)  
157 x 1110 m (north/south) at these latitudes, for analysis using Geographical Information System  
158 (GIS) applications (Fig. 2b). It might be expected that the size of the grid cells should be

296  
297  
298  
299 159 approximately equal to the distance that a vessel can travel between successive VMS records,  
300 160 otherwise the vessel could travel over a number of grid cells without being recorded, leading  
301 161 to bias. However, this is not the case. Instead, each VMS record is a *sample* of a vessel's  
302 162 location (a systematic sample over time) and the number of VMS observations in each grid  
303 163 cell will therefore be proportional to the amount of time the vessels have spent in that cell.  
304 164 The resolution of the spatial grid is therefore not limited by the distance that a vessel can  
305 165 travel between successive VMS records, but instead by the number of records in each grid  
306 166 cell. Because the data are essentially count data, the precision can be estimated using a  
307 167 Poisson distribution. At the current resolution, 95% of grid cells in the study area had at least  
308 168 10 VMS records (relative standard error: 32%) and the mean number of records was 47  
309 169 (relative standard error: 15%).

310  
311  
312  
313  
314  
315  
316  
317 170 [\[Figure 2 here please, at 1.5 columns wide\]](#)

318  
319 171 Bathymetry was obtained from the Irish National Seabed Survey (INSS) for the Whittard  
320 172 Canyon region (extent: 48.416 to 49.105 N; -11.505 to -9.846 E). The INSS was carried out  
321 173 between 1999 and 2005, covering the majority of the Irish marine continental area and is  
322 174 freely accessible through the Geological Survey of Ireland (GSI) at a resolution of 0.001 x  
323 175 0.001 degrees (~ 74 m by 111 m). Rugosity, a non-standardised (unitless) descriptor for  
324 176 seafloor roughness, was extracted using bathymetry data, point averaged down to VMS grid  
325 177 resolution and then analysed for correlations with VMS fishing effort. Here an Arc-Chord  
326 178 Ratio (ACR) rugosity index was derived through a dedicated toolbox developed by [Du Preez](#)  
327 179 [\(2012\)](#) on an ArcGIS platform. The advantage of an ACR rugosity index is that it decouples  
328 180 background slope from the rugosity determination using a plane of best fit, rather than a more  
329 181 traditional horizontal plane. It is scale independent, therefore, making it well suited for use  
330 182 over the complex topographical features found around the Whittard Canyon.

331  
332  
333 183 Individual canyon branch polygons were drawn up within the canyon system to further  
334 184 scrutinise variation in fishing and potential sediment remobilisation across each location. These  
335 185 polygons (Labelled: WC1–WC4 in [Fig. 2a](#)) were delineated using depth contours and distance  
336 186 from canyon branch channels. The deep ends of the canyon branch polygons were bound to the  
337 187 2000 m depth contour. The polygons' sides make a line orthogonal to depth contours where the  
338 188 contours turn most sharply, stepping down from the canyon interfluves. The upper end of the  
339 189 polygons (where not touching another polygon) are defined to be a VMS grid cell above or  
340 190 touching the 200 m contour, in order to include those VMS cells as part of that canyon branch

191 analysis. Although this approach is somewhat subjective, it is a best attempt at placing  
 192 boundaries between these complexly shaped spurs and channels. Further polygons were drawn  
 193 within these canyon branch divisions in an effort to focus on trawled areas that have the largest  
 194 effect on sediment transport into the canyon channels. One approach here was to alter the  
 195 original polygons by using a 10 hour VMS fishing contour as the inner or channel-side  
 196 boundary, in order to isolate, for analysis, the regularly fished interfluves of the original  
 197 polygon from the canyon axis. A second approach was to identify areas at the steepest limits of  
 198 fishing occurrence over slopes with greatest potential for down canyon sediment supply; these  
 199 strips are approximately 500 m wide and situated directly above areas of  $> 20^\circ$  slope. Fishing  
 200 rarely occurred anywhere steeper than a  $20^\circ$  slope angle (Fig. 3a).

201 Potential influences on the rugosity of the seabed were considered to be broad scale  
 202 geographic gradients, slope and fishing intensity. Estimates of the contributions of these  
 203 variables were made using generalized additive models (GAMs). An example of a GAM in  
 204 general form is as follows:

$$205 \quad \mu_i \equiv E(R_i); \quad g(\mu_i) = X_i\beta + S_1(x_{1i}) + S_2(x_{2i}, x_{3i}) + Ln_i S_3(x_4) + \dots \quad (1)$$

206 Where  $\mu_i$  is the expected value of the response variable  $R_i$  and  $g$  is a known, monotonic, link  
 207 function;  $X_i\beta$  represents any fully parametric components of the linear predictor while  
 208  $S_{1i,2i,3i,\dots}$  are the smooth functions of the predictor variables ( $x_{1i,2i,3i,\dots}$ );  $Ln_i$  is included here as  
 209 an example linear functional of  $s_{3i}$ , where there can be multiple or no such linear functional  
 210 terms throughout the model (Wood and Augustin, 2002; Wood, 2006; Wood, 2017).  $R_i$  here  
 211 is the interpolated rugosity value for each fished VMS grid cell. Predictors ( $x_{1i-4i}$ ) were the  
 212 latitude and longitude of each grid square (for geographic patterns), the estimated slope and  
 213 the total fishing hours. GAMs were used because they provide a flexible statistical modelling  
 214 framework for investigation of potentially nonlinear relationships, including interactions  
 215 between predictor variables. Fitted GAMs are smoothed functions through the data using  
 216 penalised regression splines, such that for example:

$$217 \quad S(x) = \sum_{i=1} f_i(x)\beta_i \quad (2)$$

218 Where the smooth function  $S$  constitutes values for the unknown parameters  $\beta_i$  and where  $f_i$   
 219 are chosen and known ‘basis functions’ on which the smoothing formulae rely on (Wood,  
 220 2006; Wood, 2017).

414  
415  
416 221 Screening of the data suggested that the data were not normally distributed. GAMs were  
417  
418 222 therefore estimated (in R package mgcv, Wood, 2017) using a log-link to reflect the log-  
419  
420 223 normal response variable. A number of models are possible given the four predictor variables  
421  
422 224 investigated. The comparisons of interest were defined as a purely geographic pattern  
423  
424 225 (predictors: latitude and longitude), a model based on just slope and fishing hours, and  
425  
426 226 models where variables were allowed to interact in pairs or with all four variables together.  
427  
428 227 Interaction terms test the hypothesis that the relationship of the response variable to a  
429  
430 228 predictor is not fixed, but depends on a further predictor or predictors. The most informative  
431  
432 229 of the alternative models was selected using the generalized cross validation (GCV) score,  
433  
434 230 with low values indicating the best model (Wood, 2017). GCV scores penalize additional  
435  
436 231 degrees of freedom, so the most complex model is not necessarily chosen as the most  
437  
438 232 informative.

436 233 [Figure 3 here please, at 1 column wide]

## 439 234 2.2. Hydrographic Observations

441  
442 235 Four branches of the Whittard Canyon were surveyed during summer 2013 (CE13008: 9–17<sup>th</sup>  
443  
444 236 June 2013) & 2016 (CE16006: 29<sup>th</sup> May–15<sup>th</sup> June 2016) on the *RV Celtic Explorer*.  
445  
446 237 Suspended Particulate Matter (SPM) was estimated from transmissometer measurements (C-  
447  
448 238 star, WET labs; 0.25 m path length, operating at 650 nm) in conjunction with hydrographic  
449  
450 239 measurements made with a CTD (Seabird SBE 911) and SBE32 rosette. Raw values (volts)  
451  
452 240 were converted to SPM ( $\mu\text{g l}^{-1}$ ) following the linear regression of beam attenuation values  
453  
454 241 and the mass of SPM obtained from filtered water samples (Wilson et al., 2015b).

455  
456 242 An assessment of the dynamical characteristics of recent trawling plumes measured was  
457  
458 243 made using vertical CTD profiles. The turbulent length scales and first order estimation of  
459  
460 244 magnitude in turbulent kinetic energy dissipation were quantified through Thorpe Length  
461  
462 245 scale ( $L_T$ ) analysis (Thorpe, 1977; Dillon, 1982). This method estimates the characteristic  
463  
464 246 length scale ( $L_T$ ) of density overturns within a CTD profile of sufficient vertical resolution  
465  
466 247 (here 0.25m CTD data was used).  $L_T$  is determined by reordering a profile of individual  
467  
468 248 density values ( $\rho_i$  at depth  $z_i$ ) into one where density increases monotonically with depth ( $\rho_i$   
469  
470 249 at depth  $z_0$ ). A corresponding profile of density displacements ( $z_i - z_0$ ) is produced.  $L_T$  is then  
471  
472 250 defined as the RMS displacement value over an appropriate averaging process. This  
473  
474 251 averaging is typically over individual overturns in a ‘packet’ of finite vertical extent where

473  
474  
475 252 the sum of the individual Thorpe displacements equals zero, and that are not associated with  
476  
477 253 instrument noise (e.g. Galbraith and Kelley, 1996; Mater et al., 2013). Furthermore, a simple  
478  
479 254 estimate of the energy dissipation ( $\epsilon$ ) can be made following the arguments of Dillon (1982)  
480  
481 255 and assuming  $L_T$  is proportional to the Ozmidov length scale,  $L_O$ , which is used to describe  
482  
483 256 the scale of turbulence in a stably stratified flow. Here we note caution in that  $L_T$  is  
484  
485 257 principally a method to estimate the vertical eddy size from the density profiles and only a  
486  
487 258 limited method to fully quantify the turbulence (e.g. Mater et al., 2013).

488 259 Assuming that  $L_T$  and  $L_O$  are proportional,  $\epsilon$  can be found from a measurement of  $L_T$ ,

489  
490 260 
$$\epsilon = 0.64 * L_T^2 * N^3 \quad (3)$$
  
491

492  
493 261 where  $N$  is the buoyancy frequency ( $N^2 = [-g/\rho_0] * d\rho/dz$ ).  
494

495 262

### 498 263 *2.3. Biogeochemical analysis of suspended particulate material*

499  
500 264 Suspended particulate organic matter (sPOM) was collected using a Stand Alone Pump  
501  
502 265 System (SAPS; Challenger Oceanic), deployed by a winch on the CTD wire or attached to  
503  
504 266 the CTD. Large volumes of water (163–1143 l) were filtered through two stacked pre-  
505  
506 267 combusted (400 °C; > 6 hrs) glass fibre GF/F (Whatman, 293 mm diameter) filters at the  
507  
508 268 surface and near bottom depths (7–22 m above the seabed). Filters were folded into quarters,  
509  
510 269 wrapped in pre-combusted aluminium foil on recovery and stored at –80 °C for the duration  
511  
512 270 of the cruise. Filters were subsequently freeze-dried and stored at –20 °C until analysis.

513  
514 271 Elemental and molecular analysis was carried out on sPOM collected from Bottom Nepheloid  
515  
516 272 Layers (BNLs) between 1310–1370 m water depth (< 20 m above the seabed) from the four  
517  
518 273 branches and a surface sample (locations: Fig. 2a). Particulate organic carbon (POC) and  
519  
520 274 particulate nitrogen (PN) were measured from punched circles (113 mm<sup>2</sup>) in homogeneous  
521  
522 275 areas at the middle and edge of the top filter only. Analyses were carried out using a  
523  
524 276 CEInstruments NC 2500 CHN analyser in duplicates and the mean value was taken. POC  
525  
526 277 values were obtained after de-carbonation of the filters (HCl vapour method; Yamamuro and  
527  
528 278 Kayanne, 1995), whereas PN values were determined without de-carbonation. Mean values  
529  
530 279 of the middle and edge filter samples were taken to eliminate filtration artefacts.  
531  
280 Concentrations below the limit of detection (< 0.01) were considered nil. Values were not

532  
533  
534 281 corrected for dissolved organic material due to the large volumes of water filtered (Moran et  
535 al., 1999).  
536 282

537  
538 283 Lipid extractions and analyses of suspended Particulate Organic Matter (sPOM) were carried  
539 out according to the methods of Kiriakoulakis et al. (2007; 2009; 2011) to determine the total  
540 284 fatty acid and alcohol content. Briefly, portions (1/4) of the SAPS filter (~ 6.21–7.75 g) were  
541 285 spiked with 20 µl of internal standard (100 ng/µl 5α(H)-Cholestane; Sigma) and extracted by  
542 286 sonication (30 min @ 30 °C; x 3) in ~ 20 ml dichloromethane:methanol (9:1). Extracts were  
543 287 later transmethylated (24 hrs; 40 °C) with 1 ml methanolic acetyl chloride (30:1) and  
544 288 derivatised with 50 µl of *bis*-trimethylsilyltrifluoroacetamide (BSFTA, 1%  
545 289 trimethylsilylchloride; Stigma; 30 min @ 40 °C). Extracts were stored at –20 °C until  
546 290 analysis.  
547 291

548 292 GC-MS analysis was carried out using a Varian 450 Gas Chromatographer Mass  
549 293 Spectrometer. Extracts were run in batches and loaded onto the column (Agilent VF-MS  
550 294 column: 30 m x 0.25 mm, 0.25 µm; carrier gas helium @ 1 mL min<sup>-1</sup>) using a CP8400  
551 295 autosampler and a CP-1177 split/splitless injector. The column was fed directly into the  
552 296 electron (EI) source of a Saturn 220 mass spectrometer (ionisation potential 70 eV; source  
553 297 temperature 220 °C; trap current 300 µA; full data acquisition mode). Chromatograms were  
554 298 reviewed and processed using Varian MS Workstation software (version 6.9.1). Compounds  
555 299 were identified by comparison of their mass spectra and relative retention times with  
556 300 authentic standards (Supelco TM37 FAME mix; 47085-U; 47015-U; 47033 Sigma-Aldrich)  
557 301 using the total ion current (TIC) chromatogram. Compound concentrations were calculated  
558 302 by comparison of peak areas of the internal standard with those of the compounds of interest.  
559 303 The relative response factors of the analytes were determined individually and/or for similar  
560 304 compounds. Organic contamination in procedural blanks extracted with each sample batch  
561 305 was subtracted from the sample values. Reproducibility of similar lipid analyses was  
562 306 determined to be ± 15% by Kiriakoulakis et al. (2000). Concentrations were normalised to  
563 307 volume of water as an indicator of food availability. The contribution of phytoplankton in  
564 308 each sample was calculated by the sum of C<sub>14</sub> – C<sub>22</sub> saturated fatty alcohols (Volkman et al.,  
565 309 1998), straight chained fatty acids and C<sub>16:1(n-7)</sub> (Harwood and Russell, 1984; Conte et al.,  
566 310 2003) and PUFAs (e.g. Duineveld et al., 2012); see also supplementary information.  
567 311 Similarly, bacterial indices were calculated by the sum of C<sub>18:1n7</sub> and odd numbered saturated  
568 312 and branched fatty acids (Volkman and Johns, 1977; Duineveld et al., 2012).  
569  
570  
571  
572  
573  
574  
575  
576  
577  
578  
579  
580  
581  
582  
583  
584  
585  
586  
587  
588  
589  
590

591  
592  
593  
594  
595  
596  
597  
598  
599  
600  
601  
602  
603  
604  
605  
606  
607  
608  
609  
610  
611  
612  
613  
614  
615  
616  
617  
618  
619  
620  
621  
622  
623  
624  
625  
626  
627  
628  
629  
630  
631  
632  
633  
634  
635  
636  
637  
638  
639  
640  
641  
642  
643  
644  
645  
646  
647  
648  
649

313

### 314 **3. Results**

315

#### 316 *3.1. Bottom trawling intensity and rugosity correlation*

317 Fishing occurred up to depths of around 1300 m right across the region studied (~ 7744 km<sup>2</sup>),  
318 with fishing intensity clearly related to bathymetry and to large scale canyon features, such as  
319 interfluves or plateaux, up as far as the shelf break (Fig. 2b). The combined total time spent  
320 by the fishing industry engaging in bottom trawling was 1.46 x 10<sup>5</sup> hours or just under 17  
321 years over the 10-year period analysed. Over each VMS grid square (approximately 0.82  
322 km<sup>2</sup>) actively fished in the 10 years, the mean fishing effort was 4.8 hrs, median fishing effort  
323 was 23.4 hrs and the highest fished grid-square saw 208 hrs of bottom trawling (fishing effort  
324 from VMS having an accuracy of approximately 88% after Gerritsen and Lordan, 2011). The  
325 highest bottom fishing values were found out along the interfluves and plateaux adjacent to  
326 steeper slopes. Although concentrated on lower slopes and shallower waters, fishing effort  
327 regularly occurred on steeper inclines (> 10°) on canyon flanks around the edges of  
328 interfluves and occasionally in waters deeper than 1000 m. As of December 2016, deep-sea  
329 bottom trawling below 800 m deep is prohibited in these waters by EU law (EU 2016/2336).

330 **[Figure 4 here please, at 1 column wide]**

331 In an effort to assess the most appropriate type of analysis, an initial plot of rugosity against  
332 slope was constructed with fishing points split between high and low around their median (Fig.  
333 4). This identified the non-linear nature of the dataset, where the relationship between slope  
334 and rugosity may be different with different levels of fishing activity. High levels of fishing  
335 only occurred on low slopes and less complex rugosity, whereas low levels of fishing  
336 occurred over the whole region considered. Further examination of the data suggested that the  
337 calculated variation in rugosity among grid squares was lower in more heavily fished areas.  
338 This pattern changed with slope (Fig. 5). By splitting the rugosity values into heavily and  
339 lightly fished grid squares (using median fishing effort: 23.4 hrs), standard deviation of  
340 rugosity can be summarized for each subset, and viewed as a proxy for heterogeneity of  
341 seafloor roughness. For shallower slopes there was no difference between high and low

650  
651  
652 342 fished grid squares, but at higher slopes the more heavily fished areas had less variation in  
653  
654 343 rugosity (roughness) values.

655  
656 344 [Figure 5 here please, at 1 column wide, with black and white for print and colour for online  
657  
658 345 viewing]

660  
661 346 There was statistical evidence for location, slope and fishing intensity all being related to  
662 347 changes in rugosity (Table 1). Judged by GCV scores, models with only two variables were  
663  
664 348 inferior to a model that contained all four predictors (comparing models 1–3). Allowing all  
665 349 four variables to interact (model 4) did not improve predictive value compared to the model  
666  
667 350 where all variables had independent effects (model 3). A model with terms where slope and  
668  
669 351 fishing interacted, along with a geographic interaction (model 6), had the lowest GCV score  
670 352 and highest adjusted- $R^2$  of the alternative models. This can therefore be viewed as the most  
671  
672 353 informative summary of the relationships between variables.

673  
674 354 [Table 1 here please]

675  
676  
677 355 The geographic effect (Fig. 6a) is a general decrease in rugosity with increasing latitude, with  
678 356 some variation in the rate of change with longitude, as is expected in this area going from  
679  
680 357 deep canyon to shelf. Independent of the geographic pattern, rugosity contours show  
681  
682 358 increasing roughness with steeper slopes (Fig. 6b). The interaction with fishing intensity  
683 359 indicated a local increase in rugosity for low slope areas (particularly between 30 and 100  
684  
685 360 fishing hours), reflected in the deflection of the fitted contour at low slopes. For example, the  
686  
687 361 average rugosity on seabed with less than 0.5 degree slope was 1.0048 (SE 0.00011) between  
688 362 40 and 70 VMS hours and 1.0045 (SE 0.00011) at all other VMS values. Rugosity contours  
689  
690 363 for areas with slopes steeper than 10° suggested that rugosity decreased with increased  
691 364 fishing. This pattern can be interpreted by comparing areas with low and high fishing effort  
692  
693 365 for the same slope value. For example, at zero fishing, the predicted residual variation  
694 366 rugosity is above 0.005 on a 10° slope; at 50 fishing hours residual rugosity was predicted to  
695  
696 367 be below 0.005 at the same slope value.

697  
698 368 [Figure 6 here please, at 1 column wide]

699  
700  
701 369 An east-west variation in fishing intensity was discovered across the four main canyon  
702 370 branches studied (WC1–WC4). Due to its geometry and the distribution of fishing intensity  
703  
704 371 around that channel, WC4 was the largest probable contributor to down-slope sediment flux;

709  
710  
711 372 followed by WC3 (Table 2). WC2 and WC1 to the west contributed least. By focussing on  
712 373 the interfluves flanking the WC4 canyon branch channel, the largest fishing intensity per area  
713 374 (79.6 hrs km<sup>-2</sup> over the 10 years) was identified out of the whole region. There was very little  
714 375 fishing occurring on slopes greater than 20°, consequently this was chosen as a boundary  
715 376 between slopes fished and not fished. As with individual canyon branch results, these focused  
716 377 areas (Table 2), such as ones fished just above slopes of 20°, displayed a steady west to east  
717 378 increase (~ 5.3 hrs km<sup>-2</sup>) in fishing intensity.

722  
723 379 [Table 2 here please]

### 724 380 3.2. Sediment plumes within the canyon channels.

725  
726 381 Trawling, whilst modifying the seabed, also generated sources of suspended material at the  
727 382 shelf edge adjacent to the branches of the Whittard system. Sediment plumes had been  
728 383 observed in branches WC3 and WC4 during the 2013 survey (Wilson et al., 2015a). Since  
729 384 those reported observations, further plumes have been observed in the WC2 and WC4  
730 385 branches during a subsequent survey in 2016. Both the along canyon and mid-water  
731 386 conditions due to trawling plume activity were apparent from vertical profiles of 10m  
732 387 averaged derived SPM concentrations (Fig. 7). Under what were considered typical  
733 388 conditions (i.e. no trawling plumes evident), Benthic Nepheloid Layers (BNLs) of thickness  
734 389 100–200 m have SPM concentrations within a canyon branch similar to that of corresponding  
735 390 surface plankton layers (0.15–0.4 mg l<sup>-1</sup>, hatched shading in Fig. 7a). The highest values  
736 391 occurred at bottom depths associated with boundary currents or internal wave energy  
737 392 enhancement (Wilson, 2015b). The immediate aftermath of what was considered a trawling  
738 393 plume event in WC4 resulted in an increase in benthic layer SPM concentrations, in excess of  
739 394 1 mg l<sup>-1</sup>, throughout the entire length of the canyon branch that was sampled (Fig. 7b).  
740 395 Maximum BNL SPM concentration was 8 mg l<sup>-1</sup> within the mid-canyon section.  
741 396 Furthermore, values in excess of 0.3 mg l<sup>-1</sup>, found over small spatial extents at certain depths  
742 397 in normal conditions, now occupied the lower 200–400 m adjacent to the seabed along the  
743 398 entire >45 km of the canyon branch surveyed.

744  
745  
746  
747 399 [Figure 7 here please, at 1.5 columns wide]

748  
749 400 Under non-trawling plume conditions, individual vertical profiles of density and derived SPM  
750 401 showed a bottom boundary layer region from 1300 m to 15 mab (metres above seabed)  
751 402 marked by a step in the density gradient (Fig. 8a). No well-defined bottom mixed density

768  
769  
770 403 layer was apparent in the profile shown in Fig. 8a, although often present in other vertical  
771  
772 404 density profiles. An overall stratified layer up to 600 m depth was present above the bottom  
773  
774 405 layer, associated with the depth range at, or adjacent to, the permanent thermocline (Fig. 8a).  
775 406 The mid water layers contained small vertically homogeneous/near homogeneous density  
776  
777 407 layers, including reversals in the density gradient, of vertical extent 1–10 m. A BNL in the  
778  
779 408 lower 50 m of the water column is associated with a peak value of SPM reaching  $1 \text{ mg l}^{-1}$   
780 409 (Fig. 8b). A subsequent vertical profile made five days later at the same location indicated a  
781  
782 410 much more turbid BNL with a peak value of  $7.7 \text{ mg l}^{-1}$  (the axis scale truncates the plume),  
783  
784 411 but with a significant increase in background (mid water) SPM concentrations from  $\sim 1200 \text{ m}$   
785  
786 412 depth, or  $\sim 170 \text{ mab}$ . This high concentration BNL was associated with a well-mixed bottom  
787  
788 413 density layer capped by a pycnocline of density difference  $\sim 0.05 \text{ kg m}^{-3}$  (Fig. 8f).

789 414 Associated with the vertical profiles of density and SPM, individual Thorpe density  
790  
791 415 displacements in mid water occurred with magnitude up to 1–5 m over small vertical extents,  
792  
793 416 with an increase in the magnitude of displacement packets below 1000 m (Fig. 8c). A large  
794  
795 417 overturn was highlighted between 1200–1300 m, with maximum displacements peaking at 30  
796  
797 418 m immediately above the bottom boundary region. For the plume event, similar mid water  
798  
799 419 characteristics in Thorpe displacements were again present but with a significant increase in  
800  
801 420 amplitude per overturn region below 1150 m. Increased amplitude in displacements (up to 20  
802  
803 421 m) between 1200–1300 m were associated with the upper of the two-layer BNL and  
804  
805 422 maximum displacements immediately above the seabed.  $L_T$  values up to 2 m were found  
806  
807 423 between depths 600–1000 m, with values increasing to  $\sim 5 \text{ m}$  below 1000 m and a peak of 12  
808  
809 424 m associated with the upper layer of the BNL (Fig. 8d). Corresponding values of the  
810  
811 425 turbulent kinetic energy dissipation ( $\epsilon$ ) indicated that the small mid water overturns had  
812  
813 426 values of  $\epsilon$  between  $10^{-9}$ – $10^{-8} \text{ W kg}^{-1}$  for the typical (pre-plume) scenario (Fig. 8e). The large  
814  
815 427 overturn immediately above the BBL/BNL was slightly larger ( $3 \times 10^{-8} \text{ W kg}^{-1}$ ). For the  
816  
817 428 plume event,  $L_T$  values above the BNL were similar to values for a non-plume scenario, but  
818  
819 429 increased significantly below 1200 m with values of  $O(10\text{m})$  in the upper BNL and peaking  
820  
821 430 at 22 m in the lower BNL layer (Fig. 8i). Turbulent energy dissipation during the plume event  
822  
823 431 was generally larger in mid water compared to mid water conditions with no trawl plume  
824  
825 432 present, with a number of values in excess of  $10^{-8} \text{ W kg}^{-1}$  (Fig. 8j). Values peaked between  
826  
827 433 1200–1300 m in the upper BNL with  $\epsilon \sim 10^{-7} \text{ W kg}^{-1}$ .

822 434 [Figure 8 here please, at 2 columns wide]

827  
828  
829 435 A second example of a trawling plume (from the 2013 survey), showed a plume that occurred  
830  
831 436 at a depth above the BBL, presumably the plume reaching equilibrium density before the  
832  
833 437 seabed was reached (Fig. 9). This profile was made 30 hours after one in the same location  
834  
835 438 which indicated no enhanced BNL concentration layer, and suggested a plume was captured  
836  
837 439 by the CTD profile near the end of the plume event. The main plume was centred at 1200 m  
838  
839 440 (water depth was 1370 m), about 100 m thick, with SPM concentration peaking at 5 mg l<sup>-1</sup>,  
840  
841 441 over an order of magnitude larger than non-plume BNL values (Fig. 9b). Individual overturns  
842  
843 442 and displacements were fewer in number than in the previous example but generally larger in  
844  
845 443 scale (30–40 m in vertical extent with displacements peaking at 15–20 m (e.g. at 850–900 m  
846  
847 444 and 800 m, Fig. 9c). The upper boundary of the main plume was associated with a larger  
848  
849 445 overturn between 1150–1220 m and displacements up to 30 m. Turbulent energy dissipation  
850  
851 446 (Fig. 9e) was elevated for the overturns at 800, 850–900 m and for the smaller of the two  
852  
853 447 plumes at 1000–1100 m, with values close to 10<sup>-7</sup> W kg<sup>-1</sup>, or an order of magnitude larger  
854  
855 448 than the typical mid water values associated with small overturns. The main plume overturn  
856  
857 449 had a value of  $\varepsilon = 10^{-6}$  W kg<sup>-1</sup>, the maximum energy dissipation estimated from the profiles  
858  
859 450 analysed and perhaps reflecting the capture, rather than the aftermath of, the plume event.

856 451 [Figure 9 here please, at 2 columns wide]

### 860 452

### 861 453 *3.3. Variation in quality and quantity of suspended particulate material*

863 454 The SAPs sampled SPM concentrations in the four E/BNLs (1308–1370 m) varied across the  
864  
865 455 four branches (WC1–WC4; see location in Fig. 2a) with mean values of SPM = 1.01 ±0.86  
866  
867 456 mg l<sup>-1</sup> (Table 3). Highest values were detected in WC4 (2.160 mg l<sup>-1</sup>) and associated with  
868  
869 457 bottom trawling activity. Although sampled during the same period of trawl activity, lower  
870  
871 458 SPM concentrations (0.29 mg l<sup>-1</sup>) were detected in the adjacent branch (WC3). High SPM  
872  
873 459 concentrations were also detected in WC1 (SPM = 1.18 mg l<sup>-1</sup>) but were not previously  
874  
875 460 linked to bottom trawling on the western side of the canyon system. Material from the near-  
876  
877 461 surface has a molar C/N value of 6.4, typical of oceanic surface water, while C/N values from  
878  
879 462 the E/BNLs at depth ranged from 8.2–22.2 across the four branches, with the lowest values in  
880  
881 463 WC4 and highest in WC1.

880 464 Lipids (total fatty acids and alcohols) detected in suspended Particulate Organic Matter  
881  
882 465 (sPOM) across the four branches displayed complexity and heterogeneity in both their  
883  
884  
885

886  
887  
888  
889 466 composition and concentration (Fig. 10 & Table 3). As four of the five filters were torn on  
890 467 recovery (a sampling artefact) and POC may have passed through onto the second filter,  
891  
892 468 concentrations are normalised to volume of water filter ( $\text{ng l}^{-1}$ ) here rather than OC content  
893 469 for a more reliable interpretation. The number of individual compounds identified differed  
894  
895 470 greatly, with material from the east showing less complexity ( $16 \pm 6$  V  $34 \pm 17$  individual  
896 471 compounds). Total lipid concentrations across the four branches, ranged between 181.5–  
897 472 1301.9  $\text{ng l}^{-1}$  (Fig. 10), with higher values found on the eastern side of the system. As a  
898 473 reference point, the concentration of total lipids in the near surface was 1510.4  $\text{ng l}^{-1}$ ,  
900 474 comparable to those in the east ( $1092.3 \pm 296.4 \text{ ng l}^{-1}$ ), while concentrations in the west were  
901 475 twice as low ( $349.3 \pm 237.3 \text{ ng l}^{-1}$ ).

904  
905 476 [Table 3 here please]

906  
907  
908 477 Variability in the principal lipid classes (saturated fatty acids, MUFAs, PUFAs and fatty  
909 478 alcohols) was evident (Fig. 10). Fatty acids ranged from C14 to C22 (see supplementary  
910 479 information for most commonly identified compounds). Saturated fatty acids and MUFAs  
911 480 were well represented across the four samples and accounted for  $34.8 \pm 12.0\%$  and  $34.6$   
912 481  $\pm 22.6\%$ . PUFAs represented  $< 16.9\%$ , except in the surface ( $36.8\%$ ). The greatest variance in  
913 482 dominant lipid class was observed in the alcohols, ranging from 1.8–50.8% with a mean of  
914 483  $3.4 \pm 2.3\%$  in the western (WC1 & 2) and  $46.5 \pm 6.1\%$  in eastern branches (WC3 & 4).

915  
916  
917  
918  
919  
920 484 Although PUFAs were rare, particularly in eastern branches, lipid biomarkers of  
921 485 phytoplankton origin accounted for  $93.43 \pm 0.7\%$  of the total lipids in WC3 and WC4. In  
922 486 comparison WC1 & WC2 had lower concentrations with  $68.12 \pm 9.9\%$  of the total lipids  
923 487 represented by compounds that indicated phytoplankton origin. Near-surface waters showed  
924 488 lower percentages of phytoplankton markers than any of the samples at depth ( $78.3\%$ ).

925  
926  
927  
928 489 All samples showed some level of bacterial reworking in the lipid signatures ( $4.4 \pm 2.6\%$ ).  
929 490 Bacterial biomarkers followed the opposite pattern to the phytoplankton markers, with higher  
930 491 mean values in the western branches ( $6.4 \pm 1.9$ ) and lower in the eastern ( $2.5 \pm 1.3\%$ ), further  
931 492 indicating that material in the eastern branches is more recently suspended/transported and  
932 493 fresher.

933  
934  
935  
936  
937 494 [Figure 10 here please, at 1.5 columns wide]

938  
939  
940 495

#### 496 4. Discussion

949  
950 497

951  
952  
953 498 Based on a contemporary snapshot (last 10 years) of an area where fishermen have pushed  
954 499 out into deeper fishing grounds, fishing intensity was found to be variable across the Whittard  
955 Canyon (Fig. 2). Highest fishing intensity was generally associated with smoother  
956 500 morphology, especially over steeper sloping parts of canyon interfluves (Fig. 3). The trawling  
957 501 vessels used were only limited by the physical constraints of their gear and slopes greater  
958 502 than 15° (> 1300 hrs in 10 years) were regularly fished, but rarely over slopes > 20° (90 hrs  
959 503 in 10 years). Trawling along the continental margin immediately to the east of Whittard  
960 504 Canyon is seasonal, with most fishing occurring between July and March with a maximum in  
961 505 August (Sharples et al., 2013). Due to the considerable width of the Celtic Shelf and large  
962 506 distances from the nearest fishing ports, and to the size and complexity of the Whittard  
963 507 Canyon, the canyon does not endure the same localised fishing intensity or working weekday  
964 508 cycles found at other submarine canyons more connected to coastal regions, e.g. along the  
965 509 NW Mediterranean shelf edge (e.g. Palanques et al., 2006).  
966 510

967 511 It can be estimated that grounds at Whittard are fished an average of 1.7 times per year by  
968 512 isolating the grounds most frequently fished as those above 800 m (an area of 4456 km<sup>2</sup>).  
969 513 This value was derived from a fishing effort of 1.37 x10<sup>4</sup> hrs per year, a trawl speed of 5.5  
970 514 km hr<sup>-1</sup> (Pilskaln et al., 1998; O'Neill and Summerbell, 2011) and a typical door spread of  
971 515 100 m for deep water fishing (Gerritsen et al., 2013; Payo-Payo et al., 2017). Assuming a re-  
972 516 suspended mass of 1.6 kg m<sup>-2</sup> of fished area (Oberle et al., 2016), a first order estimate of  
973 517 7.13 Mt total sediment per year may be mobilised and potentially available to enter the  
974 518 Whittard system via trawling. Notwithstanding the approximations and assumptions made  
975 519 here, this estimate highlights the ability for anthropogenic forcing to alter natural sediment  
976 520 flux, especially in areas in proximity to steep slopes with potential for triggering sediment  
977 521 gravity flows (Palanques et al., 2006; Martín et al., 2014c). Focusing on individual branches,  
978 522 ground over the flanks of WC4 were found to be fished 2.6 times the regional average,  
979 523 affording it the greatest potential for remobilising substrate. Using fishing intensity (Table 2),  
980 524 an approximation of re-suspended sediment at WC4 can be estimated (this time for 'fishing  
981 525 intensity', after O'Neill and Summerbell (2011), as opposed to 'fished area') of 9.54 x 10<sup>5</sup>  
982 526 tonne yr<sup>-1</sup>. Even if a large proportion of this suspended material resettles locally there remains  
983  
984  
985  
986  
987  
988  
989  
990  
991  
992  
993  
994  
995  
996  
997  
998  
999  
1000  
1001  
1002  
1003

1004  
1005  
1006 527 the potential for large quantities of material to be transported down canyon to deeper waters.  
1007  
1008 528 These rough estimates and to a lesser extent those for WC3 and WC1 & 2 further west, have  
1009  
1010 529 implications for generation of sediment gravity flows (Martín et al., 2014a), ENLs (Wilson et  
1011  
1012 530 al., 2015a), as well as a changing seafloor geomorphology. Traditional studies of sediment  
1013  
1014 531 flux across continental margins must take these anthropogenic affects into consideration,  
1015  
1016 532 especially in canyons, such as Whittard, which are more prone to a net export flux of  
1017  
1018 533 pelagically derived organic material, (natural or anthropogenic), due to large distance from  
1019  
1020 534 riverine sources (Oberle et al., 2016).

1020 535 Our results provide a statistical interpretation of the relationship between bottom trawling and  
1021  
1022 536 seafloor roughness in the vicinity of a large terrestrially distant submarine canyon system,  
1023  
1024 537 using a rugosity index independent of slope. Rugosity varies across many scales and in doing  
1025  
1026 538 so moderates benthic habitat at similar scales (Wilson et al., 2007; Dunn and Halpin, 2009).  
1027  
1028 539 As with slope angle (20°), rugosity is a physical constraint to bottom trawling but it has  
1029  
1030 540 proven challenging to constrain a rugosity cut-off point for fishing activity. The Whittard  
1031  
1032 541 Canyon area is likely enduring the same effects from seafloor ploughing as those found at La  
1033  
1034 542 Fonera Canyon in the NW Mediterranean by Puig et al. (2012) albeit at a slower rate and  
1035  
1036 543 wider geographical area. The GAMs analysis highlighted a complex association between  
1037  
1038 544 VMS fishing effort and rugosity (Table 1 & Fig. 6b). Where fishing activity occurred on  
1039  
1040 545 steeper slopes, there were areas of less complex rugosity than would be expected in the  
1041  
1042 546 absence of fishing. A cause and effect relationship, i.e. whether fishing vessels seek out  
1043  
1044 547 sloping areas of lower complexity or whether the activity of fishing has reduced complexity  
1045  
1046 548 in slope areas where active, could not be established. Results here, however, are in line with  
1047  
1048 549 other studies (e.g. Puig et al., 2012; Payo-Payo et al., 2017). In this respect, future work is  
1049  
1050 550 planned to focus on cause of seabed alteration in Whittard by conducting a ‘before and after’  
1051  
1052 551 analysis of previous (Irish National Seabed Survey, INSS) and new multibeam bathymetric  
1053  
1054 552 surveys and correlating those results with VMS data.

1050 553 Significant trawling induced sediment plumes are generated within the canyon channels of the  
1051  
1052 554 Whittard system, remnants of which have been observed in light transmission profiles of up to  
1053  
1054 555 200 m thick adjacent to the seabed (Fig. 7). Such anthropogenic sourced sediment plumes had  
1055  
1056 556 been suggested to occur in Whittard Canyon previously (Wilson et al., 2015a), and there is  
1057  
1058 557 undisputed evidence for them in a number of canyons at the NW Mediterranean continental  
1059  
1060 558 margin (e.g. La Fonera Canyon (Martín et al., 2014b)). Trawling induced plumes are,  
1061  
1062

1063  
1064  
1065 559 therefore, another mechanism for creating down canyon sediment flows to add to those  
1066  
1067 560 generated by naturally occurring processes, such as storm wave mobilisation of sediment (Xu  
1068  
1069 561 et al., 2004), tidally generated (Lee et al., 2009), or riverine flood events (Khripounoff et al.,  
1070  
1071 562 2009). The intensity and prolonged seasonal timeframe of fishing activity, however, implies  
1072  
1073 563 that the anthropogenically generated plumes will provide a significant contribution to the  
1074  
1075 564 integrated export flux at continental margin sites.

1076 565 The sediment gravity flows observed here are energetic, with an estimated turbulent energy  
1077  
1078 566 dissipation ( $\varepsilon$ ) an order of magnitude greater than for benthic nepheloid layers that occur  
1079  
1080 567 under background conditions, despite the observations being made post event (Figs. 8, 9).  
1081  
1082 568 Values in  $\varepsilon$  up to  $10^{-6}$  W kg<sup>-1</sup> were estimated from Thorpe length scale analysis of density  
1083  
1084 569 overturns in CTD profiles. The use of Thorpe length scale is a simple and indirect method to  
1085  
1086 570 determine  $\varepsilon$  (e.g. Mater et al., 2013), with additional errors in absolute values related to the  
1087  
1088 571 small number of overturns sampled here (e.g. MacDonald et al., 2013). Furthermore,  $\varepsilon$  is  
1089  
1090 572 dependent on the variability of  $L_T$  with Ozmidov length scale  $L_o$ , and  $L_T$  probably represents  
1091  
1092 573 the turbulent kinetic energy level more than the dissipation (Mater et al., 2015); also mean  
1093  
1094 574 values should be treated with caution. Notwithstanding this, the dissipation values of  $\varepsilon$  appear  
1095  
1096 575 reasonable in magnitude even if estimated from a few profiles. The dissipation values found  
1097  
1098 576 here are comparable to those estimated from similar analysis, although through different  
1099  
1100 577 forcing conditions. For example, in Gaoping Canyon a value of order  $10^{-8}$  W kg<sup>-1</sup> (Lee et al.,  
1101  
1102 578 2009) was found using the Thorpe displacement method,  $\sim 2 \times 10^{-6}$  W kg<sup>-1</sup> with maximum  
1103  
1104 579 Thorpe displacements of 30 m. In the head of Monterey Canyon Gregg et al. (2005),  
1105  
1106 580 correcting previous values found in upper Monterey canyon using microstructure  
1107  
1108 581 measurements (Carter and Gregg, 2002), estimated values of  $\varepsilon \sim 1.97 \times 10^{-7}$  W kg<sup>-1</sup>, but  
1109  
1110 582 attributed this to tidal mixing.

1106 583 The values found, however, do suggest the fact that the plume events were associated with  
1107  
1108 584 enhanced turbulent kinetic energy, and keep material in suspension for extended periods of  
1109  
1110 585 time. This was observed in the aftermath of a trawl event in WC4, with enhanced SPM  
1111  
1112 586 concentrations apparent over a large vertical range throughout the canyon section (e.g. Fig. 7).  
1113  
1114 587 The increase in overturn scale and dissipation values in mid water also highlight the  
1115  
1116 588 possibility that intermediate nepheloid layers may be generated as remobilised sediment  
1117  
1118 589 enters the channel from the interfluves where trawling is most intense (Fig. 2b). The elevated  
1119  
1120 590 dynamics associated with such gravity flows will also allow detachment of sediment laden  
1121

1122  
1123  
1124 591 water from the main plumes away from the bottom boundary, such as those observed in La  
1125  
1126 592 Fonera Canyon at a bottom depth of ~ 600 m (Martín et al., 2014c). Evidence for that in  
1127  
1128 593 Whittard comes from the observation of a turbid layer immediately above the bottom  
1129  
1130 594 boundary and generally elevated turbulent energy in mid water during the event highlighted in  
1131 595 Fig. 8. Trawl induced plumes measured in 2013 in WC3 and WC4 were found in water depths  
1132  
1133 596 associated with the mid canyon reaches that had steepest canyon walls, which would promote  
1134 597 gravity flows from the adjacent interfluves (Wilson et al., 2015a). The generation of thick  
1135  
1136 598 BNLs and INLs, together with elevated turbulent energy levels within the water column,  
1137 599 suggests that material will be kept in suspension for longer and that interpretation of  
1138  
1139 600 BNL/INL sources, drivers and distribution patterns are likely to be anthropogenically  
1140 601 influenced.

1142  
1143 602 The impacts of potentially introducing even a small fraction of the 7.13 Mt sediment per year,  
1144  
1145 603 suspended by bottom trawling activities into the canyon system cannot be overlooked. The  
1146 604 area of the northern Bay of Biscay has high primary productivity, in the region of 200 gC m<sup>-2</sup>  
1147  
1148 605 yr<sup>-1</sup> (Wollast and Chou, 2001). Organic carbon burial has been estimated at 0.05 g m<sup>-2</sup> yr<sup>-1</sup> at  
1149 606 the upper slope break of the Goban Spur and 0.11 g m<sup>-2</sup> yr<sup>-1</sup> further down slope (van Weering  
1150  
1151 607 et al., 1998). Perhaps, the high energy density plumes induced by trawl activity can exceed  
1152 608 the natural export of recently deposited material from the shelf and slope (Wollast, 1998).  
1153  
1154 609 From a climate perspective, the anthropogenic enhancement of sediment transport off shelf to  
1155  
1156 610 the deeper margin below the permanent thermocline, and hence out of reach from  
1157 611 atmospheric influence, has implications for long term carbon sequestration (e.g. Holt et al.,  
1158  
1159 612 2009).

1160  
1161 613 Whittard canyon, like many other submarine canyons, hosts rich biodiversity (e.g. De Leo  
1162  
1163 614 2010; Vetter et al., 2010). Diverse communities of benthic and suspension feeding fauna (Fig.  
1164  
1165 615 11) seek refuge and utilise the enhanced food input that is sustained by the canyon  
1166 616 morphology (Huvenne et al., 2011; Johnson et al., 2013). It would seem likely that adding  
1167  
1168 617 such volumes of material will have an influence on the natural biogeochemical status of  
1169 618 sinking, food rich particles in the deep-sea (Billet et al., 1983). Some studies have even  
1170  
1171 619 suggested that anthropogenic modification by trawling can have greater effects than seasonal  
1172  
1173 620 input of carbon (Sañé et al., 2013).

1174  
1175 621 While Duineveld et al. (2001) and Amaro et al. (2015) also reported episodic events  
1176  
1177 622 transporting substantial amounts of SPM, the cause of these events was not identified. SPM  
1178  
1179  
1180

1181  
1182  
1183 623 concentrations in the two eastern branches (WC3 & 4) varied dramatically ( $1.2 \pm 1.3 \text{ mg l}^{-1}$ )  
1184  
1185 624 as well as the OC content and C/N ratios ( $51.2 \pm 40.8\%$ ;  $13.8 \pm 8$  respectively). However, the  
1186  
1187 625 lipid composition from WC3 & 4 was remarkably similar; with SFAs and alcohols  
1188  
1189 626 dominating in both samples (SFAs:  $36.8 \pm 1.4\%$ ; Alcohols:  $46.5 \pm 6.1\%$ ) (Fig. 10). Contrary to  
1190  
1191 627 that found by Amaro et al. (2015), here many of the individual compounds identified have  
1192  
1193 628 phytoplankton origins ( $> 90\%$ ) and are a good food source to canyon communities within the  
1194  
1195 629 eastern branches. Furthermore, C/N values in WC4 were comparable to surface values ( $7.3$   
1196  
1197 630  $\pm 1.3$ ), and suggested that at least some of the material is fresh and has been rapidly  
1198  
1199 631 transported to this depth (1370 m) within the canyon. It is likely these compounds are utilised  
1200  
1201 632 before reaching the channel of the system (Amaro et al., 2015). The lipid composition from  
1202  
1203 633 the western branches was notably different and had dramatically lower alcohol content ( $3.4$   
1204  
1205 634  $\pm 2.3\%$ ) and higher contributions of both MUFAs ( $53.5 \pm 8.9\%$ ) and PUFAs ( $10.3 \pm 9.3\%$ )  
1206  
1207 635 (Fig. 10). Huvenne et al. (2011) also reported differences in their lipid compositions between  
1208  
1209 636 different branches, albeit the samples were also collected at different depths. They attributed  
1210  
1211 637 differences in the contributions of PUFAs (in the east) and MUFAs (in the west) to variations  
1212  
1213 638 in the contributions from phytoplankton and zooplankton from/at distinct locations and this  
1214  
1215 639 may also be the case here. However, our results would suggest that anthropogenic loading  
1216  
1217 640 should also to be considered when interpreting the biogeochemical signatures within a multi-  
1218  
1219 641 channel system, particularly given the regional variation in fishing intensity.

1214  
1215 642 Other studies have also found differences between western and eastern branches of the  
1216  
1217 643 canyon systems in faunal community compositions and abundance (Gunton et al. (2015) and  
1218  
1219 644 references within) and in sediment characteristics (Duros et al., 2011; 2012; Hunter et al.,  
1220  
1221 645 2013) and have been related to physical dynamics. Recent modelling and glider observations  
1222  
1223 646 (Amaro et al., 2016; Aslam et al., 2017) have shown that the heterogeneity of benthic  
1224  
1225 647 dynamics within Whittard Canyon is large with highly variable energy fluxes (in direction  
1226  
1227 648 and magnitude) across the various branches. Trawling may input more material into the  
1228  
1229 649 system and high energy plumes may transport fresh material from shelf regions to greater  
1230  
1231 650 depths within the canyon, but local dynamics in each branch will also influence the local  
1232  
1233 651 material transport and spatial heterogeneity in the canyon biogeochemistry. Furthermore, the  
1234  
1235 652 biogeochemical data presented here only show a snap shot in time. Indeed, although low  
1236  
1237 653 concentrations of SPM were detected at the site in WC3 (Fig 2. Sample point: S3), the  
1238  
1239 654 sampling date (14<sup>th</sup> June 2013) coincided with the detection of trawl induced ENLs in as  
655 defined by Wilson et al. (2015a) in this branch. Given this and the high C/N values, these

1240  
1241  
1242  
1243 656 measurements may be from the remnants of a trawl plume. The initial particle loading and  
1244 657 duration since the passage of a trawling plume event will determine the biogeochemical  
1245  
1246 658 composition of the suspended organic material, which further explains the highly  
1247 659 heterogenous C/N values measured here and in ENLs by [Wilson et al. \(2015a\)](#).  
1248

1249  
1250 660 Together with the geographic distribution of fishing activity, compositional differences  
1251 661 between organic material from western and eastern branches suggest that there may be a  
1252  
1253 662 zonal trend in anthropogenically introduced sediment supply. However further work is  
1254  
1255 663 needed, as there was a lack of replicates and the limited number of samples presented here,  
1256 664 does not allow for robust statistical analysis of any relationship or difference. There were no  
1257  
1258 665 statistically significant results for any of the two-sample T-tests (assuming unequal variances)  
1259 666 performed, but there were strong indications that there was a difference between  
1260  
1261 667 contributions of some lipid groups, (e.g. alcohols  $t = -9.3$ ,  $p = 0.07$ ). Other studies have  
1262  
1263 668 suggested that lipids are too labile to examine this question ([Sañé et al., 2013](#)), but here we  
1264 669 have shown that lipids may be used as sensitive biomarkers and may provide greater insight  
1265  
1266 670 into the alteration of organic material in the canyon by natural and/or trawling processes.  
1267

1268 671 [\[Figure 11 here please, at 2 columns wide\]](#)  
1269

1270  
1271 672 Alterations to the food source may have positive and negative implications depending on the  
1272 673 species feeding mechanism/habitat (e.g. [Billett et al., 1983](#); [Ramirez-Llodra et al., 2005](#);  
1273  
1274 674 [Quattrini et al., 2015](#) and references within). Increased input into the system may favour  
1275  
1276 675 suspension feeding fauna/fauna living on walls, while benthic organisms may be victim to a  
1277 676 food source with less bioavailability and higher degradation at the seabed. [Figure 11](#) presents  
1278  
1279 677 a set of photo images, in order to visualise the varying conditions experienced by local fauna.  
1280 678 Species that are accustomed to low sedimentation rates would be forced to endure any extra  
1281  
1282 679 deposition introduced by trawl fishing. These are often slow growing and/or niche species  
1283  
1284 680 susceptible to minor changes in their environment. Although these images cannot infer any  
1285 681 impacts from anthropogenic events, they do portray the wide variation of sedimentary  
1286  
1287 682 settings found. Anthropogenically generated heterogeneity in sediment supply and character  
1288 683 will also impact on habitat suitability for resident ecosystems and associated habitat niche  
1289  
1290 684 modelling ([Davies et al., 2014](#); [Robert et al., 2015](#)).

1291  
1292 685  
1293  
1294  
1295  
1296  
1297  
1298

1299  
1300  
1301 686 In recent times, the adverse effects of pollution have been realised within the marine realm,  
1302  
1303 687 for example, from offshore hydrocarbon drill cuttings on delicate cold-water coral habitats  
1304  
1305 688 (Purser and Thomsen, 2012). Toxic compounds, such as trace metals (e.g. Palanques et al.,  
1306 689 2008; Heimbürger et al., 2012; Sousa et al., 2012), along with general marine litter (Tubau et  
1307  
1308 690 al., 2015), especially micro-plastics, are being increasingly discovered on continental shelves,  
1309  
1310 691 margins and canyons. If trawling induced plumes can induce enhanced sediment flux across  
1311 692 the margin, then equally they have the capacity to accelerate the spread of other  
1312  
1313 693 anthropogenic processes, such as contamination, from shelf to deep ocean regions. This  
1314 694 anthropogenic forcing can be accentuated even further by the funnelling effect of submarine  
1315  
1316 695 canyons like those found at Whittard Canyon, even when located some distance from the  
1317 696 coastal zone.  
1318  
1319  
1320 697

## 1322 698 **5. Acknowledgments**

1323  
1324  
1325 699  
1326  
1327

1328 700 This work received support from the Griffiths Project and the Irish Centre for Research in  
1329  
1330 701 Applied Geoscience (iCRAG) through Science Foundation Ireland (SFI). The authors would  
1331 702 like to thank the captain, crews and scientists involved in CE13008 & CE16006. These  
1332  
1333 703 cruises were funded through the Marine Institute's National Shiptime Programme. The  
1334 704 authors gratefully acknowledge Sabena Blackbird (UoL) & Nicola Dempster (LJMU) for  
1335  
1336 705 their technical assistance with elemental and GC-MS analysis & Emma L. Smith (LJMU) for  
1337  
1338 706 her lipid biomarker discussions. The authors thank two anonymous reviewers for their  
1339 707 comments which significantly improved the later version of the manuscript.  
1340  
1341  
1342 708

## 1343 709 **6. References**

1344  
1345 710

- 1347 711 Amaro, T., de Stigter, H., Lavaleye, M., Duineveld, G., 2015. Organic matter enrichment in  
1348 712 the Whittard Channel; its origin and possible effects on benthic megafauna. *Deep Sea*  
1349 713 *Research Part I: Oceanographic Research Papers* 102, 90–100.  
1350 714 <https://doi.org/10.1016/j.dsr.2015.04.014>  
1351 715 Amaro, T., Huvenne, V.A.I., Allcock, A.L., Aslam, T., Davies, J.S., Danovaro, R., De  
1352 716 Stigter, H.C., Duineveld, G.C.A., Gambi, C., Gooday, A.J., Gunton, L.M., Hall, R.,  
1353 717 Howell, K.L., Ingels, J., Kiriakoulakis, K., Kershaw, C.E., Lavaleye, M.S.S., Robert, K.,  
1355  
1356  
1357

1358  
1359  
1360  
1361  
1362  
1363  
1364  
1365  
1366  
1367  
1368  
1369  
1370  
1371  
1372  
1373  
1374  
1375  
1376  
1377  
1378  
1379  
1380  
1381  
1382  
1383  
1384  
1385  
1386  
1387  
1388  
1389  
1390  
1391  
1392  
1393  
1394  
1395  
1396  
1397  
1398  
1399  
1400  
1401  
1402  
1403  
1404  
1405  
1406  
1407  
1408  
1409  
1410  
1411  
1412  
1413  
1414  
1415  
1416

- 718 Stewart, H., Van Rooij, D., White, M., Wilson, A.M., 2016. The Whittard Canyon – A  
719 case study of submarine canyon processes. *Progress in Oceanography* 146, 38–57.  
720 <https://doi.org/10.1016/j.pocean.2016.06.003>
- 721 Aslam, T., Hall, R., Dye, S., 2017. Internal tides in a dendritic submarine canyon. *Progress in*  
722 *Oceanography*. [IN PRESS]
- 723 Benn, A.R., Weaver, P.P., Billet, D.S., Van Den Hove, S., Murdock, A.P., Doneghan, G.B.,  
724 Le Bas, T., 2010. Human activities on the deep seafloor in the North East Atlantic: an  
725 assessment of spatial extent. *PloS one* 5, e12730.
- 726 Billett, D., Lampitt, R., Rice, A., Mantoura, R., 1983. Seasonal sedimentation of  
727 phytoplankton to the deep-sea benthos. *Nature* 302, 520–522.
- 728 Canals, M., Puig, P., de Madron, X.D., Heussner, S., Palanques, A., Fabres, J., 2006.  
729 Flushing submarine canyons. *Nature* 444, 354–357.
- 730 Carter, G.S., Gregg, M.C., 2002. Intense, variable mixing near the head of Monterey  
731 Submarine Canyon. *Journal of Physical Oceanography* 32, 3145–3165.
- 732 Conte, M., Dickey, T., Weber, J., Johnson, R., Knap, A., 2003. Transient physical forcing of  
733 pulsed export of bioreactive material to the deep Sargasso Sea. *Deep Sea Research Part*  
734 *I: Oceanographic Research Papers* 50, 1157–1187.
- 735 Davies, J.S., Howell, K.L., Stewart, H.A., Guinan, J., Golding, N., 2014. Defining biological  
736 assemblages (biotopes) of conservation interest in the submarine canyons of the South  
737 West Approaches (offshore United Kingdom) for use in marine habitat mapping. *Deep*  
738 *Sea Research Part II: Topical Studies in Oceanography* 104, 208–229.  
739 <https://doi.org/10.1016/j.dsr2.2014.02.001>
- 740 Davies, A.J., Roberts, J.M., Hall-Spencer, J., 2007. Preserving deep-sea natural heritage:  
741 emerging issues in offshore conservation and management. *Biological Conservation*  
742 138, 299–312.
- 743 De Leo, F.C., Smith, C.R., Rowden, A.A., Bowden, D.A., Clark, M.R., 2010. Submarine  
744 canyons: hotspots of benthic biomass and productivity in the deep sea. *Proceedings of*  
745 *the Royal Society of London B: Biological Sciences* rspb20100462.
- 746 Dillon, T., 1982. Vertical overturns: A comparison of Thorpe and Ozmidov length scales.  
747 *Journal of Geophysical Research: Oceans* 87, 9601–9613.
- 748 Doney, S.C., 2010. The growing human footprint on coastal and open-ocean  
749 biogeochemistry. *science* 328, 1512–1516.
- 750 Du Preez, C., 2015. A new arc-chord ratio (ACR) rugosity index for quantifying three-  
751 dimensional landscape structural complexity. *Landscape ecology* 30, 181.
- 752 Duineveld, G., Lavaleye, M., Berghuis, E., De Wilde, P., 2001. Activity and composition of  
753 the benthic fauna in the Whittard Canyon and the adjacent continental slope (NE  
754 Atlantic). *Oceanologica Acta* 24, 69–83.
- 755 Duineveld, G.C., Jeffreys, R.M., Lavaleye, M.S., Davies, A.J., Bergman, M.J., Watmough,  
756 T., Witbaard, R., 2012. Spatial and tidal variation in food supply to shallow cold-water  
757 coral reefs of the Mingulay Reef complex (Outer Hebrides, Scotland). *Marine Ecology*  
758 *Progress Series* 444, 97–115.
- 759 Dunn, D., Halpin, P., 2009. Rugosity-based regional modeling of hard-bottom habitat.  
760 *Marine Ecology Progress Series* 377, 1–11. <https://doi.org/10.3354/meps07839>
- 761 Duros, P., Fontanier, C., de Stigter, H.C., Cesbron, F., Metzger, E., Jorissen, F.J., 2012. Live  
762 and dead benthic foraminiferal faunas from Whittard Canyon (NE Atlantic): Focus on

1417  
1418  
1419 763 taphonomic processes and paleo-environmental applications. *Marine Micropaleontology*  
1420 764 94–95, 25–44. <https://doi.org/10.1016/j.marmicro.2012.05.004>  
1421  
1422 765 Duros, P., Fontanier, C., Metzger, E., Pusceddu, A., Cesbron, F., de Stigter, H.C., Bianchelli,  
1423 766 S., Danovaro, R., Jorissen, F.J., 2011. Live (stained) benthic foraminifera in the  
1424 767 Whittard Canyon, Celtic margin (NE Atlantic). *Deep Sea Research Part I:*  
1425 768 *Oceanographic Research Papers* 58, 128–146. <https://doi.org/10.1016/j.dsr.2010.11.008>  
1426  
1427 769 Eastwood, P.D., Mills, C.M., Aldridge, J.N., Houghton, C.A., Rogers, S.I., 2007. Human  
1428 770 activities in UK offshore waters: an assessment of direct, physical pressure on the  
1429 771 seabed. *ICES J Mar Sci* 64, 453–463. <https://doi.org/10.1093/icesjms/fsm001>  
1430 772 (EU) Council Regulation 2016/2336 of 14<sup>th</sup> December 2016 establishing specific conditions  
1431 773 for fishing for deep-sea stocks in the north-east Atlantic and provisions for fishing in  
1432 774 international waters of the north-east Atlantic and repealing Council Regulation (EC) No  
1433 775 2347/2002 (OJ L 354, 23.12.2016, p. 2)  
1434  
1435 776 Galbraith, P.S., Kelley, D.E., 1996. Identifying overturns in CTD profiles. *Journal of*  
1436 777 *Atmospheric and Oceanic Technology* 13, 688–702.  
1437 778 Gerritsen, H., Lordan, C., 2011. Integrating vessel monitoring systems (VMS) data with daily  
1438 779 catch data from logbooks to explore the spatial distribution of catch and effort at high  
1439 780 resolution. *ICES Journal of Marine Science* 68, 245–252.  
1440 781 <https://doi.org/10.1093/icesjms/fsq137>  
1441  
1442 782 Gerritsen, H.D., Minto, C., Lordan, C., 2013. How much of the seabed is impacted by mobile  
1443 783 fishing gear? Absolute estimates from Vessel Monitoring System (VMS) point data.  
1444 784 *ICES Journal of Marine Science* 70, 523–531.  
1445 785 Grassle, J.F., Maciolek, N.J., 1992. Deep-sea species richness: regional and local diversity  
1446 786 estimates from quantitative bottom samples. *The American Naturalist* 139, 313–341.  
1447 787 Gregg, M.C., Carter, G.S., Kunze, E., 2005. CORRIGENDUM. *Journal of Physical*  
1448 788 *Oceanography* 35, 1712–1715. <https://doi.org/10.1175/JPO2789.1>  
1449  
1450 789 Gunton, L.M., Gooday, A.J., Glover, A.G., Bett, B.J., 2015. Macrofaunal abundance and  
1451 790 community composition at lower bathyal depths in different branches of the Whittard  
1452 791 Canyon and on the adjacent slope (3500m; NE Atlantic). *Deep Sea Research Part I:*  
1453 792 *Oceanographic Research Papers* 97, 29–39. <https://doi.org/10.1016/j.dsr.2014.11.010>  
1454 793 Hall, R.A., Aslam, T., Huvenne, V.A.I., 2017. Partly standing internal tides in a dendritic  
1455 794 submarine canyon observed by an ocean glider. *Deep Sea Research Part I:*  
1456 795 *Oceanographic Research Papers*. <https://doi.org/10.1016/j.dsr.2017.05.015>  
1457  
1458 796 Halpern, B.S., Walbridge, S., Selkoe, K.A., Kappel, C.V., Micheli, F., D'Agrosa, C., Bruno,  
1459 797 J.F., Casey, K.S., Ebert, C., Fox, H.E., Fujita, R., Heinemann, D., Lenihan, H.S., Madin,  
1460 798 E.M.P., Perry, M.T., Selig, E.R., Spalding, M., Steneck, R., Watson, R., 2008. A Global  
1461 799 Map of Human Impact on Marine Ecosystems. *Science* 319, 948–952.  
1462 800 <https://doi.org/10.1126/science.1149345>  
1463  
1464 801 Harwood, J.L., Russell, N.L., 1984. *Lipids in Plants and Microorganisms*. George Allen and  
1465 802 Unwin, London.  
1466 803 Heimbürger, L.-E., Cossa, D., Thibodeau, B., Khripounoff, A., Mas, V., Chiffoleau, J.-F.,  
1467 804 Schmidt, S., Migon, C., 2012. Natural and anthropogenic trace metals in sediments of  
1468 805 the Ligurian Sea (Northwestern Mediterranean). *Chemical Geology* 291, 141–151.  
1469 806 <https://doi.org/10.1016/j.chemgeo.2011.10.011>  
1470  
1471  
1472  
1473  
1474  
1475

1476  
1477  
1478  
1479  
1480  
1481  
1482  
1483  
1484  
1485  
1486  
1487  
1488  
1489  
1490  
1491  
1492  
1493  
1494  
1495  
1496  
1497  
1498  
1499  
1500  
1501  
1502  
1503  
1504  
1505  
1506  
1507  
1508  
1509  
1510  
1511  
1512  
1513  
1514  
1515  
1516  
1517  
1518  
1519  
1520  
1521  
1522  
1523  
1524  
1525  
1526  
1527  
1528  
1529  
1530  
1531  
1532  
1533  
1534

- 807 Holt, J., Wakelin, S., Huthnance, J., 2009. Down-welling circulation of the northwest  
808 European continental shelf: A driving mechanism for the continental shelf carbon pump.  
809 *Geophysical Research Letters* 36.
- 810 Hunter, W.R., Jamieson, A., Huvenne, V.A.I., Witte, U., 2013. Sediment community  
811 responses to marine vs. terrigenous organic matter in a submarine canyon.  
812 *Biogeosciences* 10, 67–80. <https://doi.org/10.5194/bg-10-67-2013>
- 813 Huvenne, V.A., Tyler, P.A., Masson, D.G., Fisher, E.H., Hauton, C., Hühnerbach, V., Le  
814 Bas, T.P., Wolff, G.A., 2011. A picture on the wall: innovative mapping reveals cold-  
815 water coral refuge in submarine canyon. *PloS one* 6, e28755.
- 816 Johnson, M.P., White, M., Wilson, A., Würzberg, L., Schwabe, E., Folch, H., Allcock, A.L.,  
817 2013. A vertical wall dominated by *Acesta excavata* and *Neopycnodonte zibrowii*, part  
818 of an undersampled group of deep-sea habitats. *PloS one* 8, e79917.
- 819 Jones, J., 1992. Environmental impact of trawling on the seabed: a review. *New Zealand*  
820 *Journal of Marine and Freshwater Research* 26, 59–67.
- 821 Kaiser, M.J., Collie, J.S., Hall, S.J., Jennings, S., Poiner, I.R., 2002. Modification of marine  
822 habitats by trawling activities: prognosis and solutions. *Fish and Fisheries* 3, 114–136.  
823 <https://doi.org/10.1046/j.1467-2979.2002.00079.x>
- 824 Khripounoff, A., Vangriesheim, A., Crassous, P., Etoubleau, J., 2009. High frequency of  
825 sediment gravity flow events in the Var submarine canyon (Mediterranean Sea). *Marine*  
826 *Geology* 263, 1–6. <https://doi.org/10.1016/j.margeo.2009.03.014>
- 827 Kiriakoulakis, K., Blackbird, S., Ingels, J., Vanreusel, A., Wolff, G.A., 2011. Organic  
828 geochemistry of submarine canyons: The Portuguese Margin. *Deep Sea Research Part*  
829 *II: Topical Studies in Oceanography* 58, 2477–2488.  
830 <https://doi.org/10.1016/j.dsr2.2011.04.010>
- 831 Kiriakoulakis, K., Freiwald, A., Fisher, E., Wolff, G., 2007. Organic matter quality and  
832 supply to deep-water coral/mound systems of the NW European Continental Margin.  
833 *International Journal of Earth Sciences* 96, 159–170.
- 834 Kiriakoulakis, K., Marshall, J., Wolff, G., 2000. Biomarkers in a Lower Jurassic concretion  
835 from Dorset (UK). *Journal of the Geological Society* 157, 207–220.
- 836 Kiriakoulakis, K., Vilas, J.C., Blackbird, S.J., Arístegui, J., Wolff, G.A., 2009. Seamounts  
837 and organic matter—Is there an effect? The case of Sedlo and Seine seamounts, Part 2.  
838 Composition of suspended particulate organic matter. *Deep Sea Research Part II:*  
839 *Topical Studies in Oceanography* 56, 2631–2645.  
840 <https://doi.org/10.1016/j.dsr2.2008.12.024>
- 841 Koenig, S., Fernández, P., Company, J.B., Huertas, D., Solé, M., 2013. Are deep-sea  
842 organisms dwelling within a submarine canyon more at risk from anthropogenic  
843 contamination than those from the adjacent open slope? A case study of Blanes canyon  
844 (NW Mediterranean). *Progress in Oceanography* 118, 249–259.  
845 <https://doi.org/10.1016/j.pocean.2013.07.016>
- 846 Lee, I.-H., Lien, R.-C., Liu, J.T., Chuang, W., 2009. Turbulent mixing and internal tides in  
847 Gaoping (Kaoping) submarine canyon, Taiwan. *Journal of Marine Systems* 76, 383–396.
- 848 Levin, L.A., Dayton, P.K., 2009. Ecological theory and continental margins: where shallow  
849 meets deep. *Trends in ecology & evolution* 24, 606–617.
- 850 Levin, L.A., Sibuet, M., 2012. Understanding continental margin biodiversity: a new  
851 imperative. *Annual Review of Marine Science* 4, 79–112.

1535  
1536  
1537  
1538  
1539  
1540  
1541  
1542  
1543  
1544  
1545  
1546  
1547  
1548  
1549  
1550  
1551  
1552  
1553  
1554  
1555  
1556  
1557  
1558  
1559  
1560  
1561  
1562  
1563  
1564  
1565  
1566  
1567  
1568  
1569  
1570  
1571  
1572  
1573  
1574  
1575  
1576  
1577  
1578  
1579  
1580  
1581  
1582  
1583  
1584  
1585  
1586  
1587  
1588  
1589  
1590  
1591  
1592  
1593

- 852 Levin, L.A., Sibuet, M., Gooday, A.J., Smith, C.R., Vanreusel, A., 2010. The roles of habitat  
853 heterogeneity in generating and maintaining biodiversity on continental margins: an  
854 introduction. *Marine Ecology* 31, 1–5.
- 855 MacDonald, D.G., Carlson, J., Goodman, L., 2013. On the heterogeneity of stratified-shear  
856 turbulence: Observations from a near-field river plume. *Journal of Geophysical  
857 Research: Oceans* 118, 6223–6237.
- 858 Martín, J., Puig, P., Masqué, P., Palanques, A., Sánchez-Gómez, A., 2014a. Impact of bottom  
859 trawling on deep-sea sediment properties along the flanks of a submarine canyon. *PloS  
860 one* 9, e104536.
- 861 Martín, J., Puig, P., Palanques, A., Giamportone, A., 2014b. Commercial bottom trawling as  
862 a driver of sediment dynamics and deep seascape evolution in the Anthropocene.  
863 *Anthropocene* 7, 1–15. <https://doi.org/10.1016/j.ancene.2015.01.002>
- 864 Martín, J., Puig, P., Palanques, A., Masqué, P., García-Orellana, J., 2008. Effect of  
865 commercial trawling on the deep sedimentation in a Mediterranean submarine canyon.  
866 *Marine Geology* 252, 150–155.
- 867 Martín, J., Puig, P., Palanques, A., Ribó, M., 2014c. Trawling-induced daily sediment  
868 resuspension in the flank of a Mediterranean submarine canyon. *Deep Sea Research Part  
869 II: Topical Studies in Oceanography, Submarine Canyons: Complex Deep-Sea  
870 Environments Unravelling by Multidisciplinary Research* 104, 174–183.  
871 <https://doi.org/10.1016/j.dsr2.2013.05.036>
- 872 Mater, B.D., Schaad, S.M., Venayagamoorthy, S.K., 2013. Relevance of the Thorpe length  
873 scale in stably stratified turbulence. *Physics of Fluids* 25, 076604.
- 874 Mater, B.D., Venayagamoorthy, S.K., St. Laurent, L., Moum, J.N., 2015. Biases in Thorpe-  
875 scale estimates of turbulence dissipation. Part I: Assessments from large-scale overturns  
876 in oceanographic data. *Journal of Physical Oceanography* 45, 2497–2521.
- 877 Morato, T., Watson, R., Pitcher, T.J., Pauly, D., 2006. Fishing down the deep. *Fish and  
878 fisheries* 7, 24–34.
- 879 Nédélec, C., Prado, J., 1990. Definition and classification of fishing gear categories.  
880 Définition et classification des catégories d'engins de pêche. Definición y clasificación  
881 de las diversas categorías de artes de pesca. *FAO Fisheries Technical Paper*.
- 882 Oberle, F.K.J., Storlazzi, C.D., Hanebuth, T.J.J., 2016a. What a drag: Quantifying the global  
883 impact of chronic bottom trawling on continental shelf sediment. *Journal of Marine  
884 Systems* 159, 109–119. <https://doi.org/10.1016/j.jmarsys.2015.12.007>
- 885 Oberle, F.K.J., Swarzenski, P.W., Reddy, C.M., Nelson, R.K., Baasch, B., Hanebuth, T.J.J.,  
886 2016b. Deciphering the lithological consequences of bottom trawling to sedimentary  
887 habitats on the shelf. *Journal of Marine Systems* 159, 120–131.  
888 <https://doi.org/10.1016/j.jmarsys.2015.12.008>
- 889 O'Neill, F.G., Summerbell, K., 2011. The mobilisation of sediment by demersal otter trawls.  
890 *Marine Pollution Bulletin* 62, 1088–1097.  
891 <https://doi.org/10.1016/j.marpolbul.2011.01.038>
- 892 Palanques, A., 1994. Distribution and heavy metal pollution of the suspended particulate  
893 matter on the Barcelona continental shelf (North-Western Mediterranean).  
894 *Environmental Pollution* 85, 205–215.
- 895 Palanques, A., Martín, J., Puig, P., Guillén, J., Company, J.B., Sardà, F., 2006. Evidence of  
896 sediment gravity flows induced by trawling in the Palamós (Fonera) submarine canyon

1594  
1595  
1596  
1597  
1598  
1599  
1600  
1601  
1602  
1603  
1604  
1605  
1606  
1607  
1608  
1609  
1610  
1611  
1612  
1613  
1614  
1615  
1616  
1617  
1618  
1619  
1620  
1621  
1622  
1623  
1624  
1625  
1626  
1627  
1628  
1629  
1630  
1631  
1632  
1633  
1634  
1635  
1636  
1637  
1638  
1639  
1640  
1641  
1642  
1643  
1644  
1645  
1646  
1647  
1648  
1649  
1650  
1651  
1652

- 897 (northwestern Mediterranean). *Deep Sea Research Part I: Oceanographic Research*  
898 *Papers* 53, 201–214. <https://doi.org/10.1016/j.dsr.2005.10.003>
- 899 Palanques, A., Masqué, P., Puig, P., Sanchez-Cabeza, J.A., Frignani, M., Alvisi, F., 2008.  
900 Anthropogenic trace metals in the sedimentary record of the Llobregat continental shelf  
901 and adjacent Foix Submarine Canyon (northwestern Mediterranean). *Marine Geology*  
902 248, 213–227. <https://doi.org/10.1016/j.margeo.2007.11.001>
- 903 Palanques, A., Puig, P., Guillén, J., Demestre, M., Martín, J., 2014. Effects of bottom  
904 trawling on the Ebro continental shelf sedimentary system (NW Mediterranean).  
905 *Continental Shelf Research* 72, 83–98.
- 906 Payo-Payo, M., Jacinto, R., Lastras, G., Rabineau, M., Puig, P., Martín, J., Canals, M.,  
907 Sultan, N., 2017. Numerical modeling of bottom trawling-induced sediment transport  
908 and accumulation in La Fonera submarine canyon, northwestern Mediterranean Sea.  
909 *Marine Geology* 386, 107–125.
- 910 Pham, C.K., Ramirez-Llodra, E., Alt, C.H., Amaro, T., Bergmann, M., Canals, M., Davies, J.,  
911 Duineveld, G., Galgani, F., Howell, K.L., 2014. Marine litter distribution and density in  
912 European seas, from the shelves to deep basins. *PLoS One* 9, e95839.
- 913 Pilskaln, C.H., Churchill, J.H., Mayer, L.M., 1998. Resuspension of sediment by bottom  
914 trawling in the Gulf of Maine and potential geochemical consequences. *Conservation*  
915 *Biology* 12, 1223–1229.
- 916 Puig, P., Canals, M., Company, J.B., Martín, J., Amblas, D., Lastras, G., Palanques, A.,  
917 Calafat, A.M., 2012. Ploughing the deep sea floor. *Nature* 489, 286–289.  
918 <https://doi.org/10.1038/nature11410>
- 919 Puig, P., Palanques, A., Martín, J., 2014. Contemporary Sediment-Transport Processes in  
920 Submarine Canyons. *Annual Review of Marine Science* 6, 53–77.  
921 <https://doi.org/10.1146/annurev-marine-010213-135037>
- 922 Purser, A., Thomsen, L., 2012. Monitoring strategies for drill cutting discharge in the vicinity  
923 of cold-water coral ecosystems. *Marine Pollution Bulletin* 64, 2309–2316.  
924 <https://doi.org/10.1016/j.marpolbul.2012.08.003>
- 925 Pusceddu, A., Bianchelli, S., Martín, J., Puig, P., Palanques, A., Masqué, P., Danovaro, R.,  
926 2014. Chronic and intensive bottom trawling impairs deep-sea biodiversity and  
927 ecosystem functioning. *Proceedings of the National Academy of Sciences* 111, 8861–  
928 8866.
- 929 Pusceddu, A., Fiordelmondo, C., Danovaro, R., 2005a. Sediment resuspension effects on the  
930 benthic microbial loop in experimental microcosms. *Microbial ecology* 50, 602–613.
- 931 Pusceddu, A., Fiordelmondo, C., Polymenakou, P., Polychronaki, T., Tselepidis, A.,  
932 Danovaro, R., 2005b. Effects of bottom trawling on the quantity and biochemical  
933 composition of organic matter in coastal marine sediments (Thermaikos Gulf,  
934 northwestern Aegean Sea). *Continental Shelf Research* 25, 2491–2505.
- 935 Quattrini, A.M., Nizinski, M.S., Chaytor, J.D., Demopoulos, A.W.J., Roark, E.B., France,  
936 S.C., Moore, J.A., Heyl, T., Auster, P.J., Kinlan, B., Ruppel, C., Elliott, K.P., Kennedy,  
937 B.R.C., Lobecker, E., Skarke, A., Shank, T.M., 2015. Exploration of the Canyon-Incised  
938 Continental Margin of the Northeastern United States Reveals Dynamic Habitats and  
939 Diverse Communities. *PLOS ONE* 10, e0139904.  
940 <https://doi.org/10.1371/journal.pone.0139904>

1653  
1654  
1655  
1656  
1657  
1658  
1659  
1660  
1661  
1662  
1663  
1664  
1665  
1666  
1667  
1668  
1669  
1670  
1671  
1672  
1673  
1674  
1675  
1676  
1677  
1678  
1679  
1680  
1681  
1682  
1683  
1684  
1685  
1686  
1687  
1688  
1689  
1690  
1691  
1692  
1693  
1694  
1695  
1696  
1697  
1698  
1699  
1700  
1701  
1702  
1703  
1704  
1705  
1706  
1707  
1708  
1709  
1710  
1711

- 941 Ramirez-Llodra, E., Tyler, P.A., Baker, M.C., Bergstad, O.A., Clark, M.R., Escobar, E.,  
942 Levin, L.A., Menot, L., Rowden, A.A., Smith, C.R., 2011. Man and the last great  
943 wilderness: human impact on the deep sea. *PLoS One* 6, e22588.
- 944 Reid, G., Hamilton, D., 1990. A reconnaissance survey of the Whittard Sea Fan,  
945 Southwestern Approaches, British Isles. *Marine Geology* 92, 69–86.  
946 [https://doi.org/10.1016/0025-3227\(90\)90027-H](https://doi.org/10.1016/0025-3227(90)90027-H)
- 947 Robert, K., Jones, D.O.B., Tyler, P.A., Van Rooij, D., Huvenne, V.A.I., 2015. Finding the  
948 hotspots within a biodiversity hotspot: fine-scale biological predictions within a  
949 submarine canyon using high-resolution acoustic mapping techniques. *Mar Ecol* 36,  
950 1256–1276. <https://doi.org/10.1111/maec.12228>
- 951 Sanchez-Vidal, A., Canals, M., Calafat, A.M., Lastras, G., Pedrosa-Pàmies, R., Menéndez,  
952 M., Medina, R., Hereu, B., Romero, J., Alcoverro, T., 2012. Impacts on the deep-sea  
953 ecosystem by a severe coastal storm. *PLoS One* 7, e30395.
- 954 Sañé, E., Martín, J., Puig, P., Palanques, A., 2013. Organic biomarkers in deep-sea regions  
955 affected by bottom trawling: pigments, fatty acids, amino acids and carbohydrates in  
956 surface sediments from the La Fonera (Palamós) Canyon, NW Mediterranean Sea.  
957 *Biogeosciences* 10, 8093.
- 958 Sharples, J., Scott, B.E., Inall, M.E., 2013. From physics to fishing over a shelf sea bank.  
959 *Progress in Oceanography* 117, 1–8. <https://doi.org/10.1016/j.pocean.2013.06.015>
- 960 Sousa, A.C.A., Oliveira, I.B., Laranjeiro, F., Takahashi, S., Tanabe, S., Cunha, M.R.,  
961 Barroso, C.M., 2012. Organotin levels in Nazaré canyon (west Iberian Margin, NE  
962 Atlantic) and adjacent coastal area. *Marine Pollution Bulletin* 64, 422–426.  
963 <https://doi.org/10.1016/j.marpolbul.2011.11.013>
- 964 Thorpe, S., 1977. Turbulence and mixing in a Scottish loch. *Philosophical Transactions of the*  
965 *Royal Society of London A: Mathematical, Physical and Engineering Sciences* 286,  
966 125–181.
- 967 Tubau, X., Canals, M., Lastras, G., Rayo, X., Rivera, J., Amblas, D., 2015. Marine litter on  
968 the floor of deep submarine canyons of the Northwestern Mediterranean Sea: The role of  
969 hydrodynamic processes. *Progress in Oceanography* 134, 379–403.  
970 <https://doi.org/10.1016/j.pocean.2015.03.013>
- 971 Van Weering, T.C., Hall, I., De Stigter, H., McCave, I., Thomsen, L., 1998. Recent  
972 sediments, sediment accumulation and carbon burial at Goban Spur, NW European  
973 Continental Margin (47–50 N). *Progress in Oceanography* 42, 5–35.
- 974 Vetter, E.W., Smith, C.R., De Leo, F.C., 2010. Hawaiian hotspots: enhanced megafaunal  
975 abundance and diversity in submarine canyons on the oceanic islands of Hawaii. *Marine*  
976 *Ecology* 31, 183–199.
- 977 Volkman, J., Johns, R., 1977. The geochemical significance of positional isomers of  
978 unsaturated acids from an intertidal zone sediment. *Nature* 267, 693–694.
- 979 Volkman, J.K., Barrett, S.M., Blackburn, S.I., Mansour, M.P., Sikes, E.L., Gelin, F., 1998.  
980 Microalgal biomarkers: a review of recent research developments. *Organic*  
981 *Geochemistry* 29, 1163–1179.
- 982 Watling, L., Norse, E.A., 1998. Disturbance of the Seabed by Mobile Fishing Gear: A  
983 Comparison to Forest Clearcutting. *Conservation Biology* 12, 1180–1197.  
984 <https://doi.org/10.1046/j.1523-1739.1998.0120061180.x>
- 985 Wilson, A.M., Kiriakoulakis, K., Raine, R., Gerritsen, H.D., Blackbird, S., Allcock, A.L.,  
986 White, M., 2015a. Anthropogenic influence on sediment transport in the Whittard

1712  
1713  
1714 987 Canyon, NE Atlantic. *Marine Pollution Bulletin* 101, 320–329.  
1715 988 <https://doi.org/10.1016/j.marpolbul.2015.10.067>  
1716  
1717 989 Wilson, A.M., Raine, R., Mohn, C., White, M., 2015b. Nepheloid layer distribution in the  
1718 990 Whittard Canyon, NE Atlantic Margin. *Marine Geology* 367, 130–142.  
1719 991 <https://doi.org/10.1016/j.margeo.2015.06.002>  
1720 992 Wilson, M.F.J., O’Connell, B., Brown, C., Guinan, J.C., Grehan, A.J., 2007. Multiscale  
1721 993 Terrain Analysis of Multibeam Bathymetry Data for Habitat Mapping on the  
1722 994 Continental Slope. *Marine Geodesy* 30, 3–35.  
1723 995 <https://doi.org/10.1080/01490410701295962>  
1724  
1725 996 Wollast, R., 1998. Evaluation and comparison of the global carbon cycle in the coastal zone  
1726 997 and in the open ocean. *The sea* 10, 213–252.  
1727 998 Wollast, R., Chou, L., 2001. The carbon cycle at the ocean margin in the northern Gulf of  
1728 999 Biscay. *Deep Sea Research Part II: Topical Studies in Oceanography* 48, 3265–3293.  
1729  
1730 1000 Wood, S., 2017. mgcv: Mixed GAM Computation Vehicle with GCV/AIC/REML  
1731 1001 smoothness estimation.  
1732 1002 Wood, S., 2006. *Generalized Additive Models: An Introduction with R*. CRC Press.  
1733 1003 Wood, S.N., Augustin, N.H., 2002. GAMs with integrated model selection using penalized  
1734 1004 regression splines and applications to environmental modelling. *Ecological modelling*  
1735 1005 157, 157–177.  
1736  
1737 1006 Xu, J., Noble, M., Rosenfeld, L.K., 2004. In-situ measurements of velocity structure within  
1738 1007 turbidity currents. *Geophysical Research Letters* 31.  
1739 1008 Yamamuro, M., Kayanne, H., 1995. Rapid direct determination of organic carbon and  
1740 1009 nitrogen in carbonate-bearing sediments with a Yanaco MT-5 CHN analyzer.  
1741 1010 *Limnology and Oceanography* 40, 1001–1005.  
1742 1011  
1743  
1744 1012  
1745

## 1746 1013 **Figure captions**

1747  
1748 1014  
1749 1015 Fig. 1. General overview of the Celtic Margin off the northwest European Continental Shelf.  
1750  
1751 1016 The red box is Fig. 2: Whittard Canyon. Image reproduced from the GEBCO world map  
1752 1017 2014, [www.gebco.net](http://www.gebco.net)  
1753  
1754  
1755 1018 Fig. 2. Area map of Whittard Canyon: (a) showing contoured bathymetry (in blue), SPM  
1756 1019 sample location labels: Ss = surface SPM; S1–4 = SPM samples from WC1–4 and turbulent  
1757 1020 energy analysis locations: K8 (Fig. 8) & K9 (Fig. 9). (b) bathymetry overlaid with bottom  
1758 1021 trawling fishing hours from light in yellow to heavy in brown, with a minimum of 10 hrs  
1759  
1760 1021  
1761 1022 shown.  
1762  
1763  
1764  
1765  
1766  
1767  
1768  
1769  
1770

1771  
1772  
1773 1023 Fig. 3. (a) Map image of slope angle at Whittard Canyon, with areas in red being greater than  
1774 1024 20°. (b): Map image of ACR rugosity index; contours of VMS fishing effort are  
1775 1025 superimposed at 10 h (brown) and 100 h (green).  
1776  
1777  
1778  
1779 1026 Fig. 4. ACR Rugosity against slope angle for all VMS grid cells split between high (purple)  
1780 1027 and low (orange) fishing by their median.  
1781  
1782  
1783 1028 Fig. 5. Canyon branch WC3: Standard deviation of rugosity among grid cells for the heavier  
1784 1029 fished (purple) and lighter fished (orange) data points. Split between ‘heavy’ and ‘light’  
1785 1030 fishing on the basis of the median VMS fishing value. [Colour for online publishing]  
1786  
1787  
1788  
1789 1031 Fig. 5. Canyon branch WC3: Standard deviation of rugosity among grid cells for the heavier  
1790 1032 fished (solid) and lighter fished (dashed) data points. Split between ‘heavy’ and ‘light’  
1791 1033 fishing on the basis of the median VMS fishing value. [Black and white for print]  
1792  
1793  
1794  
1795 1034 Fig. 6. (a) Geographical representation of data points with contours of predicted residual  
1796 1035 variation rugosity as output by GAMs package mgcv (Wood, 2017). (b) Partial residual plot  
1797 1036 showing the combined influence of fishing effort and slope on rugosity. Contours of rugosity  
1798 1037 indicate the GAM fit to data for the whole Whittard Canyon region, controlling for the other  
1799 1038 predictors in the best model. Points indicate the distribution of observations for each  
1800 1039 predictor.  
1801  
1802  
1803  
1804  
1805 1040 Fig. 7. (a) Along channel section of SPM concentration ( $\text{mg l}^{-1}$ ) in WC4 in the immediate  
1806 1041 aftermath of a trawling plume, showing the 0.3 and 1  $\text{mg l}^{-1}$  contours only. For comparison  
1807 1042 the hatched area indicates the regions where SPM concentrations  $> 0.3 \text{ mg l}^{-1}$  were measured  
1808 1043 in other canyon branches when no trawling plumes were evident during the survey. The  
1809 1044 station locations are shown by the ‘x’. In (b), selected vertical profiles of SPM for the above  
1810 1045 section are indicated in the thick line with thin line showing examples from the same depth in  
1811 1046 unaffected branches.  
1812  
1813  
1814  
1815  
1816  
1817 1047 Fig. 8. Vertical profiles of (a)  $\sigma_t$ , (b) SPM ( $\text{mg l}^{-1}$ ), (c) Individual Thorpe displacements (m),  
1818 1048 (d) Thorpe Length Scale for overturns (m) and (e)  $\log_{10}$  of the turbulent energy dissipation ( $\epsilon$ ,  
1819 1049  $\text{W kg}^{-1}$ ), for the WC4 location at  $\sim 1380$  water depth in 2016 (see Fig. 2a; K8). (f-j) are the  
1820 1050 corresponding profiles at the same location during a plume event 31 hours later. Note in (g),  
1821 1051 the SPM scale is cut off at  $5 \text{ mg l}^{-1}$ , for clarity – the maximum value in the near bottom turbid  
1822 1052 layer was  $8 \text{ mg l}^{-1}$ .  
1823  
1824  
1825  
1826  
1827  
1828  
1829

1830  
1831  
1832  
1833 1053 Fig. 9. Vertical profiles of (a)  $\sigma_t$ , (b) SPM ( $\text{mg l}^{-1}$ ), (c) Individual Thorpe displacements (m),  
1834 1054 (d) Thorpe Length Scale for overturns (m) and (e)  $\log_{10}$  of the turbulent energy dissipation ( $\epsilon$ ,  
1835  
1836 1055  $\text{W kg}^{-1}$ ), for the WC3 location at  $\sim 1385$  water depth, 2013 (see Fig. 2a; K9).  
1837

1838 1056 Fig. 10. Map image showing concentrations of total lipids normalised to volume of water ( $\text{ng}$   
1839  $\text{l}^{-1}$ ) detected in suspended particulate organic matter collected in four branches (WC1 – 4) and  
1840 1057 at the surface of Whittard Canyon in June 2013. Pie charts show the contribution of saturated  
1841 1058 fatty acids, monounsaturated fatty acids (MUFAs), polyunsaturated fatty acids (PUFAs) and  
1842 1059 fatty alcohols in each sample (locations: S1 – 4 and surface sample Ss; see Fig. 2a).  
1843 1060  
1844  
1845 1060  
1846 1061  
1847

1848  
1849 1062 Fig. 11. Photo images from Whittard Canyon 2013 – 2016, displaying contrasting sediment  
1850 1063 concentrations both in the water column and resettling on benthic fauna. (a1): Cloudy water  
1851 surrounds a Brisingid starfish; WC3. (a2): Very clear water and a Flytrap anemone; WC1.  
1852 1064 (b1): Sediment laden *Acesta excavata*; WC3. (b2): Clean *A. excavata*; WC3. (c1): The soft  
1853 1065 coral *Anthomastus* topped with a veil of sediment; WC3. (c2): An *Anthomastus* perched on a  
1854 1066 canyon wall with polyps fully extended. Note that the *Anthomastus* (c1) with retracted polyps  
1855 1067 may have become sediment covered during earlier ROV manoeuvres adjacent to site  
1856 1068 (visibility was not sufficient to determine this from the video), but the quantity of loose  
1857 1069 sediment available for such coverage may have been introduced by trawling.  
1858 1070  
1859  
1860 1069  
1861 1070  
1862 1070  
1863  
1864 1071  
1865  
1866  
1867

## 1868 1072 Table captions

1870 1073 Table 1. Generalised Additive Model (GAM) fits to predict rugosity values in the full dataset,  
1871 excluding cells with zero fishing ( $n = 6241$  grid cells). Model predictors: R = Rugosity, Ln =  
1872 1074 longitude, Lt = Latitude, V = VMS fishing hours, S = slope angle. Variables in brackets have  
1873 1075 been modelled as interacting predictors. Generalised Cross Validation (GCV) scores indicate  
1874 the relative performance of models, with lower values indicating better fits. Adjusted  $R^2$   
1875 1076 values are a less robust indicator of model fit, but are included as their interpretation is more  
1876 1077 intuitive as an indicator of the performance of models at fitting the data.  
1877  
1878 1078  
1879  
1880 1079

1881  
1882 1080 Table 2. Fishing intensity ( $\text{hrs/km}^2$ ) for each canyon branch, showing results for whole  
1883 1081 branches and also broken down into specific areas within branch.  
1884  
1885  
1886  
1887  
1888

1889  
1890  
1891  
1892  
1893  
1894  
1895  
1896  
1897  
1898  
1899  
1900  
1901  
1902  
1903  
1904  
1905  
1906  
1907  
1908  
1909  
1910  
1911  
1912  
1913  
1914  
1915  
1916  
1917  
1918  
1919  
1920  
1921  
1922  
1923  
1924  
1925  
1926  
1927  
1928  
1929  
1930  
1931  
1932  
1933  
1934  
1935  
1936  
1937  
1938  
1939  
1940  
1941  
1942  
1943  
1944  
1945  
1946  
1947

1082 Table 3. Biogeochemical data for four samples (Locations S1 – 4; see Fig. 2a) & the surface  
1083 sample (Ss) used in this study with mean  $\pm$  standard deviation for Western and Eastern  
1084 samples. SPM: suspended particulate matter; C:N: molar carbon to nitrogen ratio; MUFA:  
1085 monounsaturated fatty acids; PUFA: polyunsaturated fatty acids. Individual compounds, lipid  
1086 group and primary biomarkers used for indices are shown in the Appendix. \* indicates torn  
1087 filters.

1088 Supplementary Table 1/Appendix: List of compounds most commonly identified in this study  
1089 with groups and their corresponding IUPAC names. Individual compounds used for the  
1090 phytoplankton and bacterial indices are indicated.

1091  
1092

Figures and Tables:

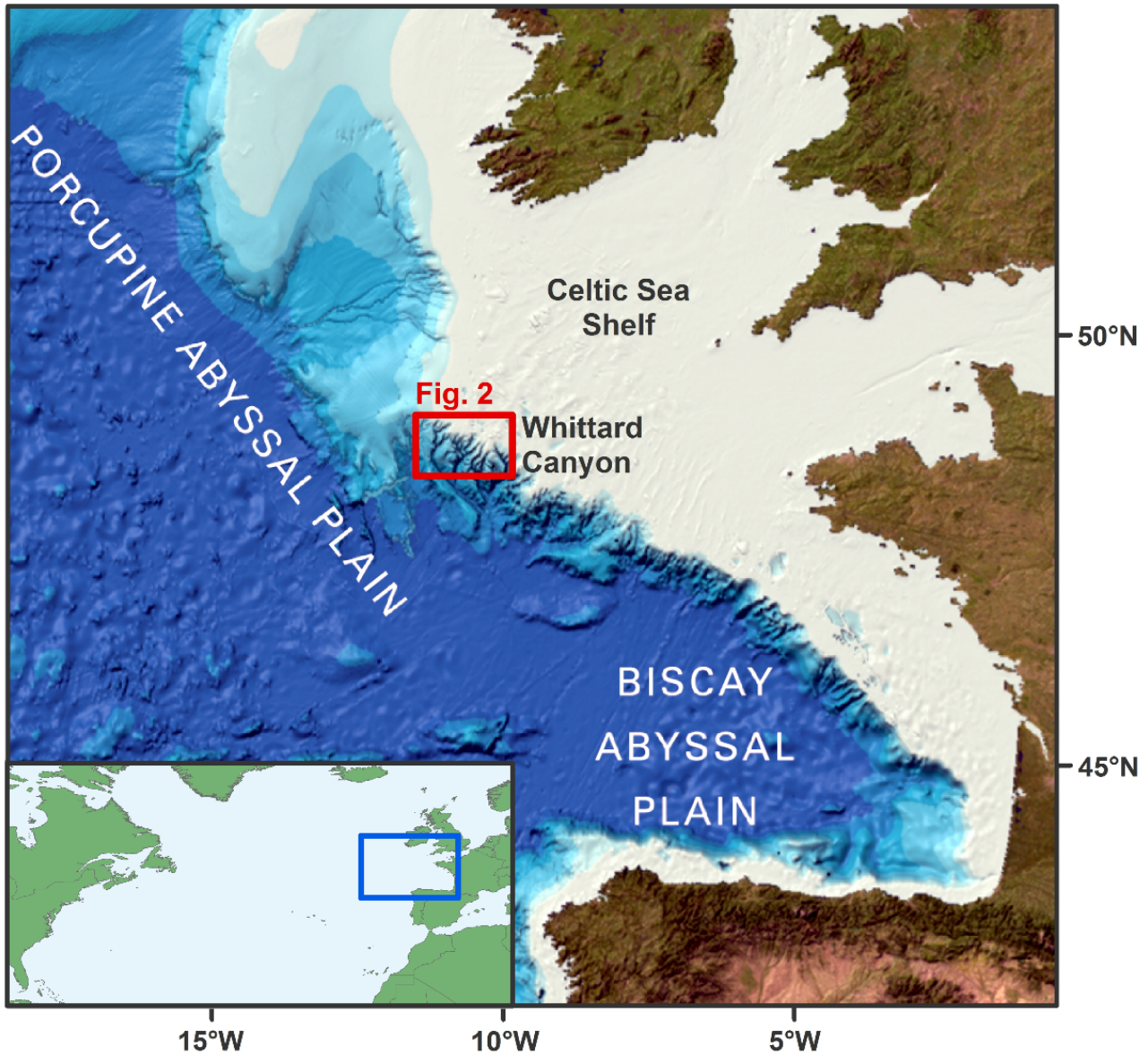


Fig. 1. General overview of the Celtic Margin off the northwest European Continental Shelf. The red box is Fig. 2: Whittard Canyon. Image reproduced from the GEBCO world map 2014, [www.gebco.net](http://www.gebco.net) [1.5 columns wide]

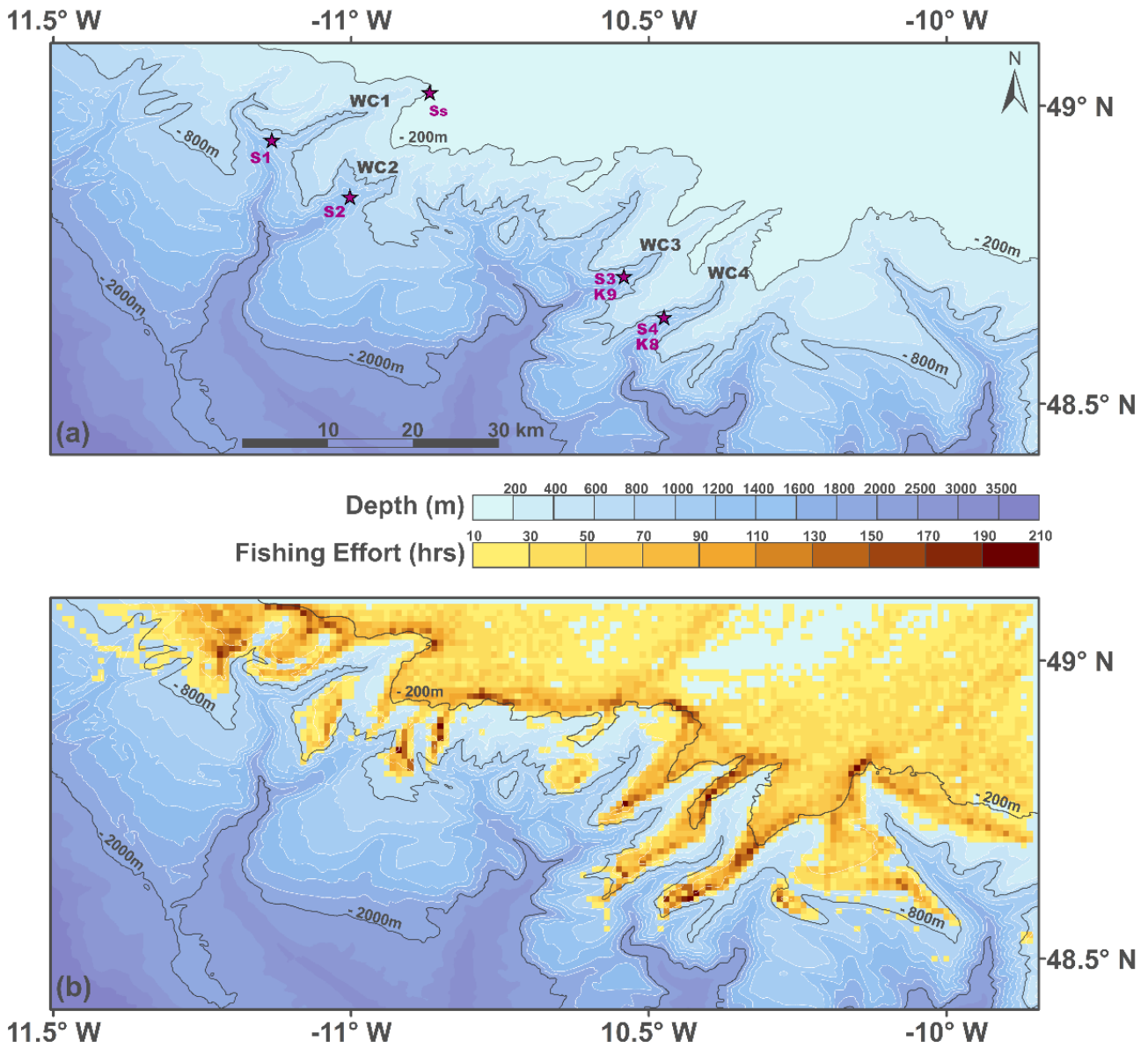


Fig. 2. Area map of Whittard Canyon: (a) showing contoured bathymetry (in blue), SPM sample location labels: Ss = surface SPM; S1–4 = SPM samples from WC1–4 and turbulent energy analysis locations: K8 (Fig. 8) & K9 (Fig. 9). (b) bathymetry overlaid with bottom trawling fishing hours from light in yellow to heavy in brown, with a minimum of 10 hrs shown. [1.5 columns wide]

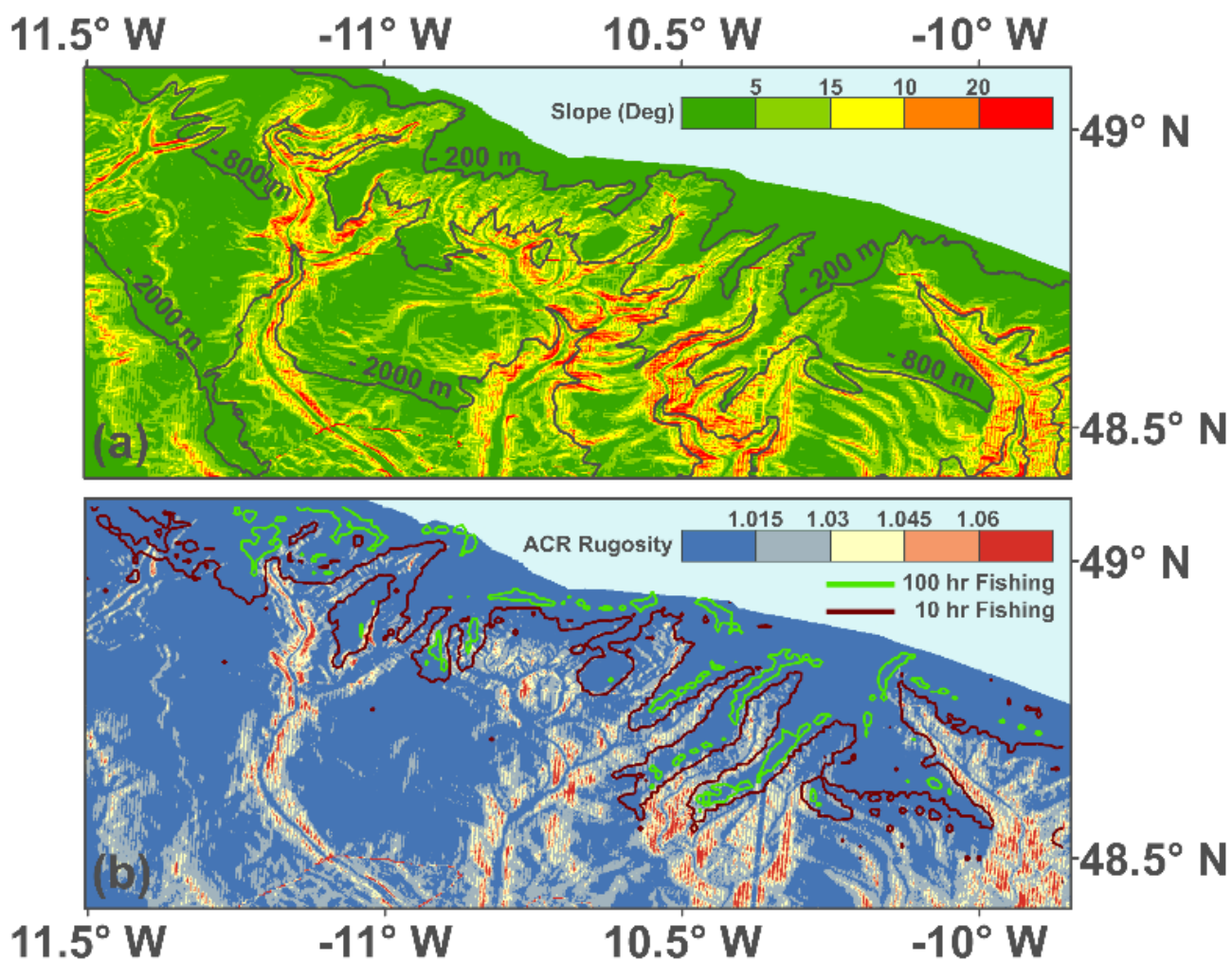


Fig. 3. (a) Map image of slope angle at Whittard Canyon, with areas in red greater than 20°. (b): Map image of ACR rugosity index; contours of VMS fishing effort are superimposed at 10 h (brown) and 100 h (green). [One column wide]

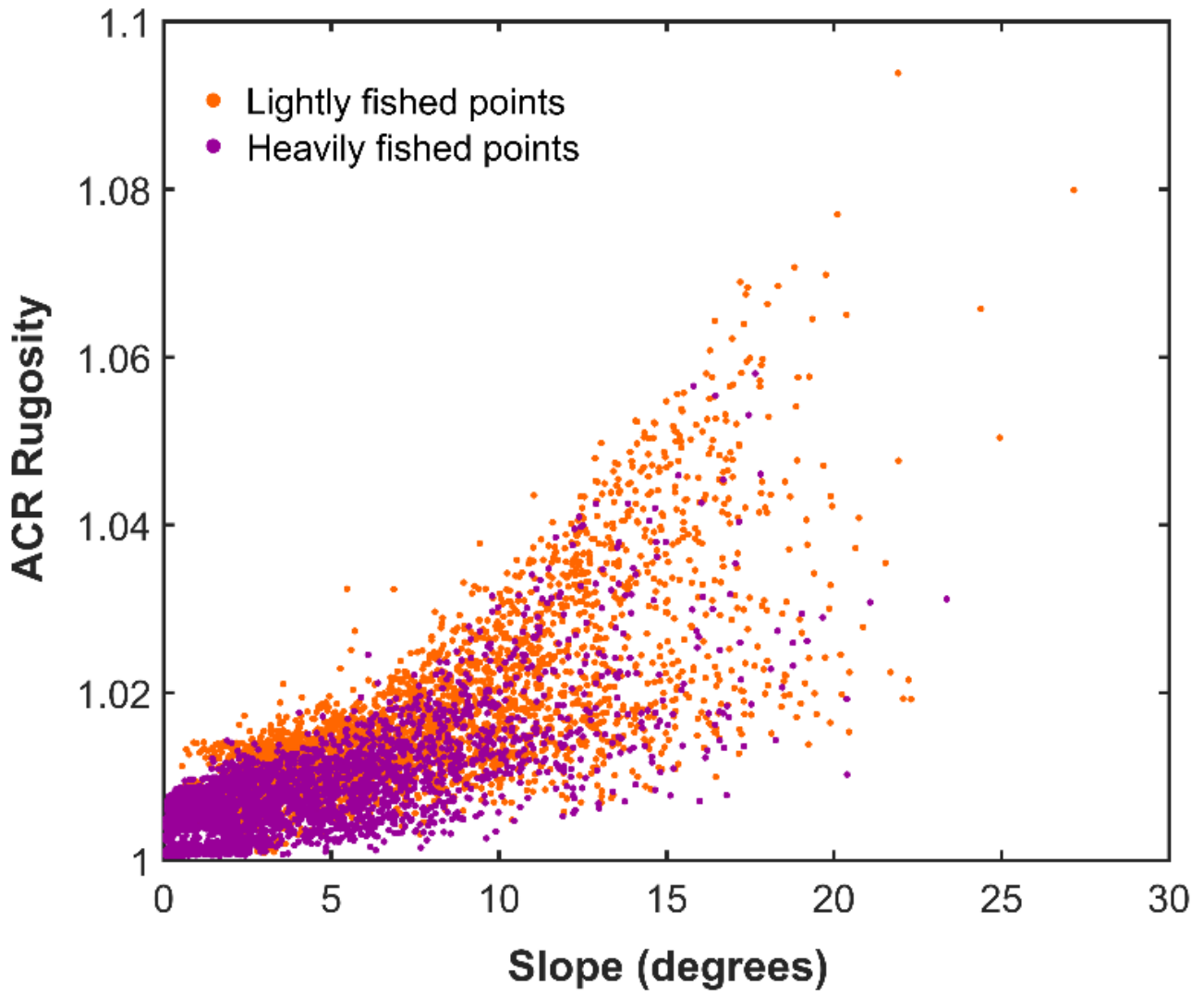


Fig. 4. ACR Rugosity against slope angle for all VMS grid cells split between high (purple) and low (orange) fishing by their median. [One column wide]

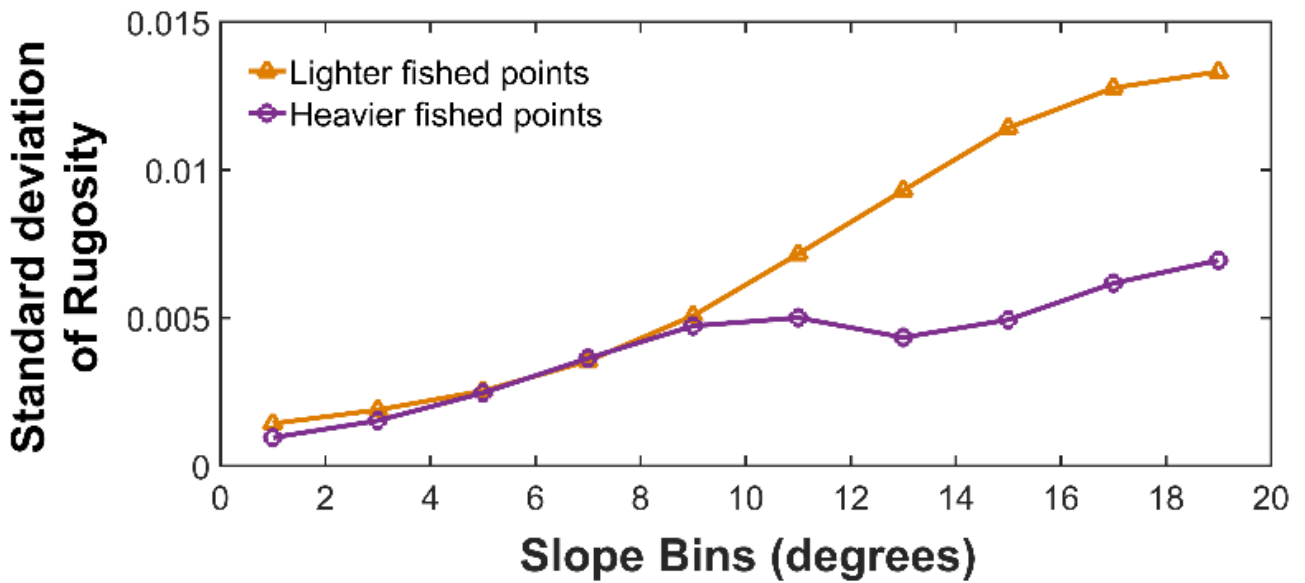


Fig. 5. Canyon branch WC3: Standard deviation of rugosity among grid cells for the heavier fished (purple) and lighter fished (orange) data points. Split between ‘heavy’ and ‘light’ fishing on the basis of the median VMS fishing value. [One column wide, for online publishing]

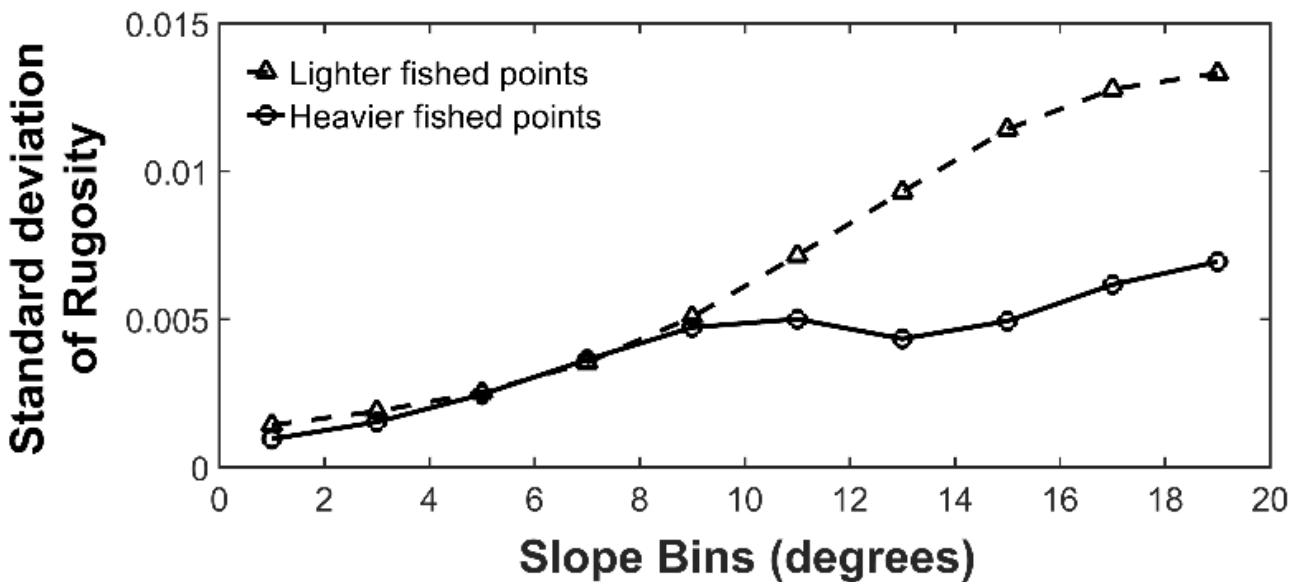


Fig. 5. Canyon branch WC3: Standard deviation of rugosity among grid cells for the heavier fished (solid) and lighter fished (dashed) data points. Split between ‘heavy’ and ‘light’ fishing on the basis of the median VMS fishing value. [One column wide, for printing]

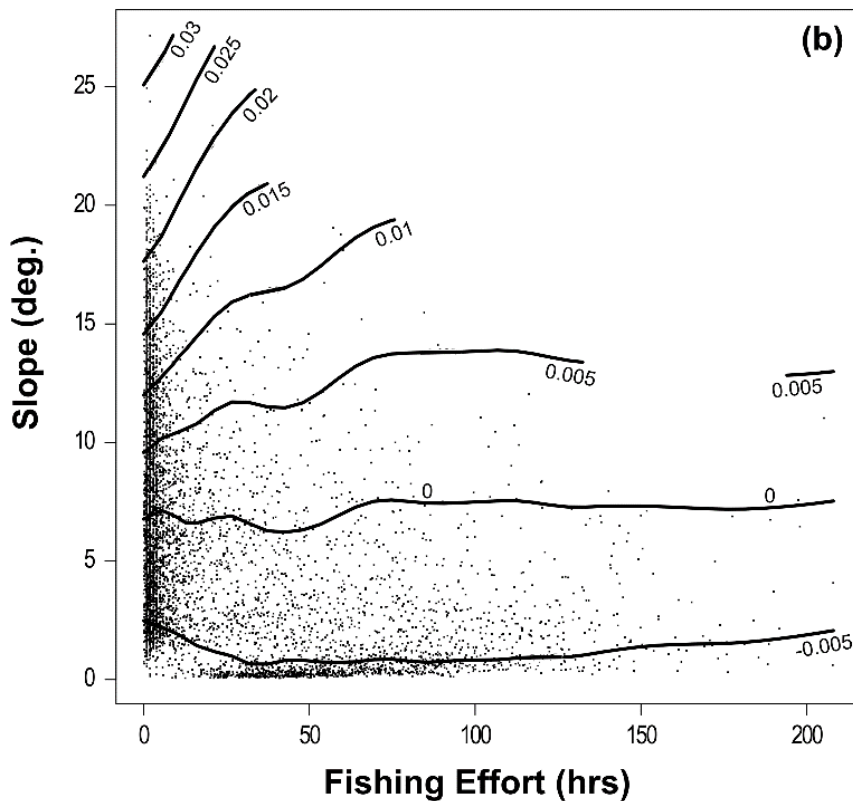
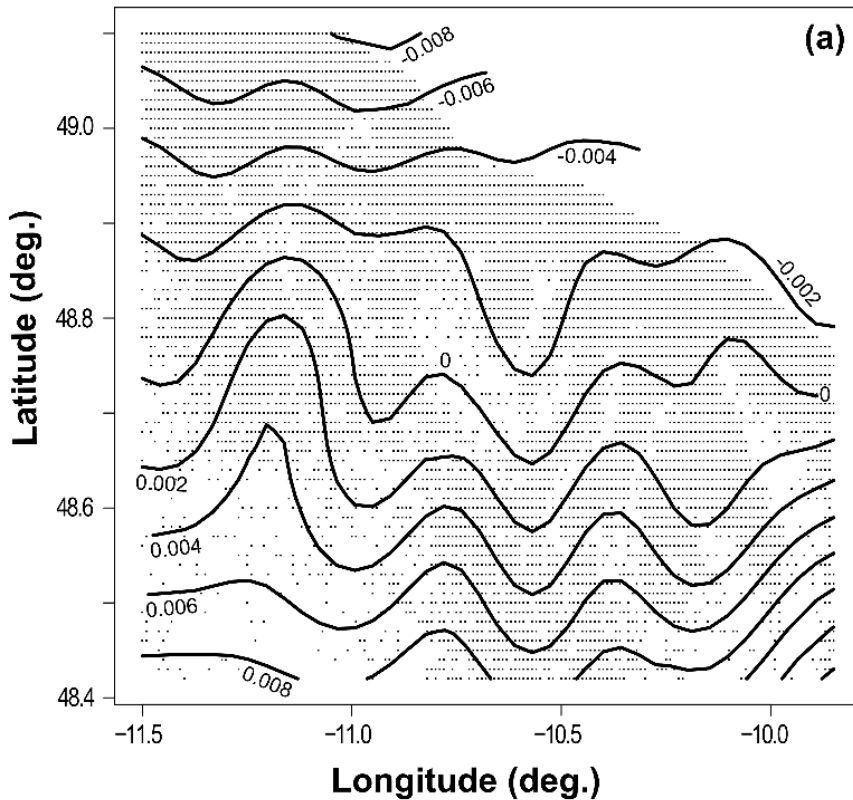


Fig. 6. (a) Geographical representation of data points with contours of predicted residual variation rugosity as output by GAMs package mgcv (Wood, 2017). (b) Partial residual plot showing the combined influence of fishing effort and slope on rugosity. Contours of rugosity indicate the GAM fit to data for the whole Whittard Canyon region, controlling for the other predictors in the best model. Points indicate the distribution of observations for each predictor. [One column wide]

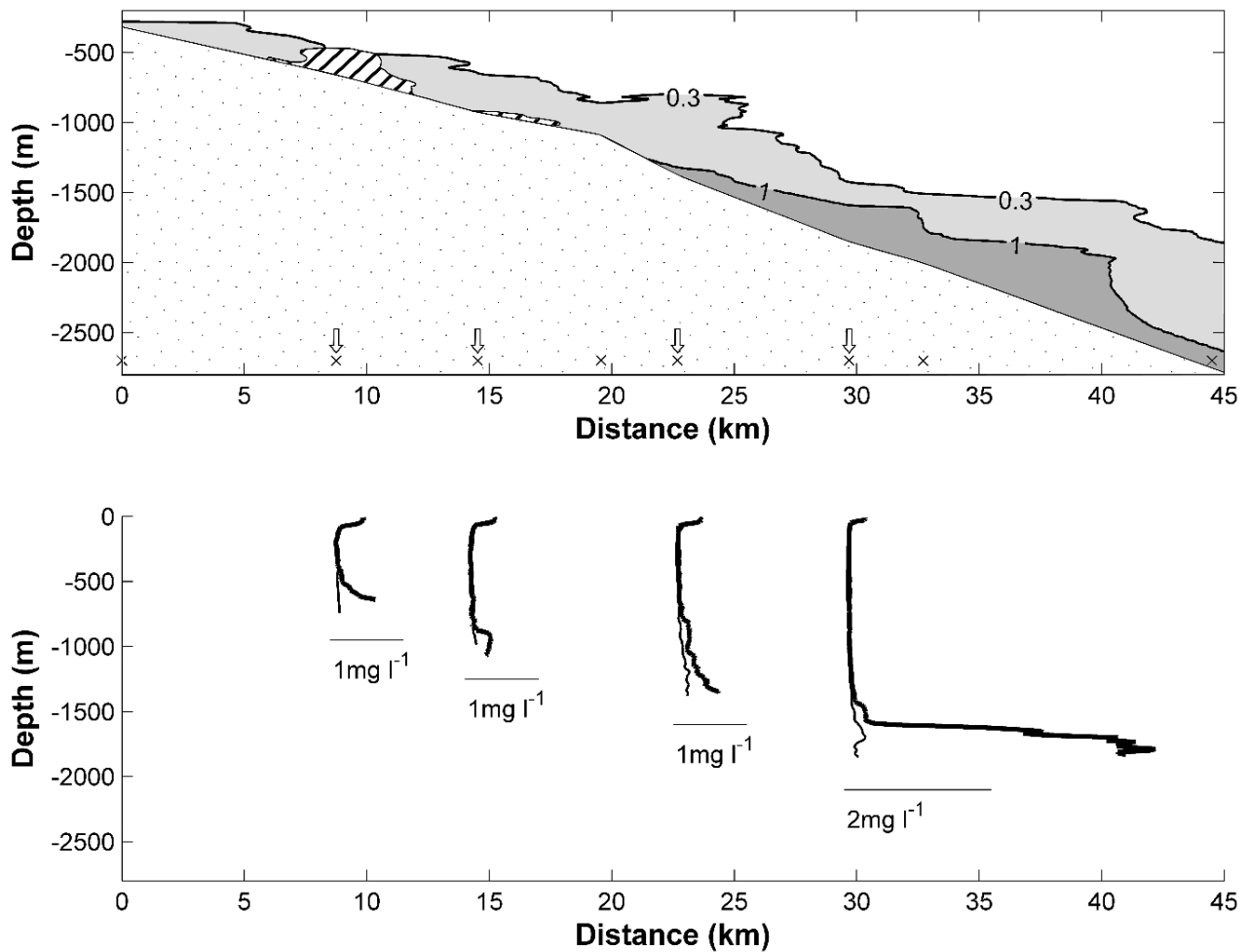


Fig. 7. (a) Along channel section of SPM concentration ( $\text{mg l}^{-1}$ ) in WC4 in the immediate aftermath of a trawling plume, showing the 0.3 and 1  $\text{mg l}^{-1}$  contours only. For comparison the hatched area indicates the regions where SPM concentrations  $> 0.3 \text{ mg l}^{-1}$  were measured in other canyon branches when no trawling plumes were evident during the survey. The station locations are shown by the 'x'. In (b), selected vertical profiles of SPM for the above section are indicated in the thick line with thin line showing examples from the same depth in unaffected branches. [1.5 columns wide]

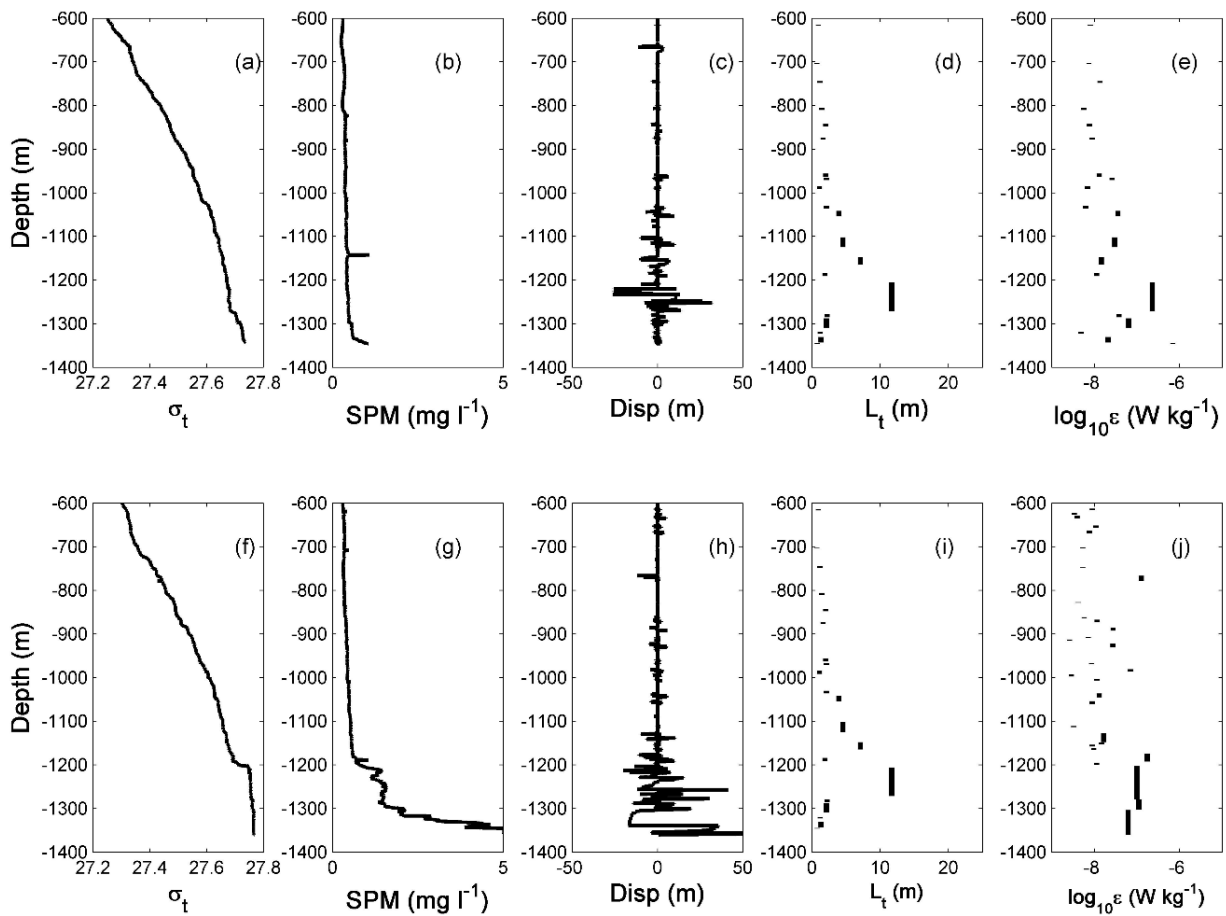


Fig. 8. Vertical profiles of (a)  $\sigma_t$ , (b) SPM ( $\text{mg l}^{-1}$ ), (c) Individual Thorpe displacements (m), (d) Thorpe Length Scale for overturns (m) and (e)  $\log_{10}$  of the turbulent energy dissipation ( $\epsilon$ ,  $\text{W kg}^{-1}$ ), for the WC4 location at  $\sim 1380$  water depth in 2016 (see Fig. 2a; K8). (f-j) are the corresponding profiles at the same location during a plume event 31 hours later. Note in (g), the SPM scale is cut off at  $5 \text{ mg l}^{-1}$ , for clarity – the maximum value in the near bottom turbid layer was  $8 \text{ mg l}^{-1}$ . [Two columns wide]

473  
474  
475  
476  
477  
478  
479  
480  
481  
482  
483  
484  
485  
486  
487  
488  
489  
490  
491  
492  
493  
494  
495  
496  
497  
498  
499  
500  
501  
502  
503  
504  
505  
506  
507  
508  
509  
510  
511  
512  
513  
514  
515  
516  
517  
518  
519  
520  
521  
522  
523  
524  
525  
526  
527  
528  
529  
530  
531

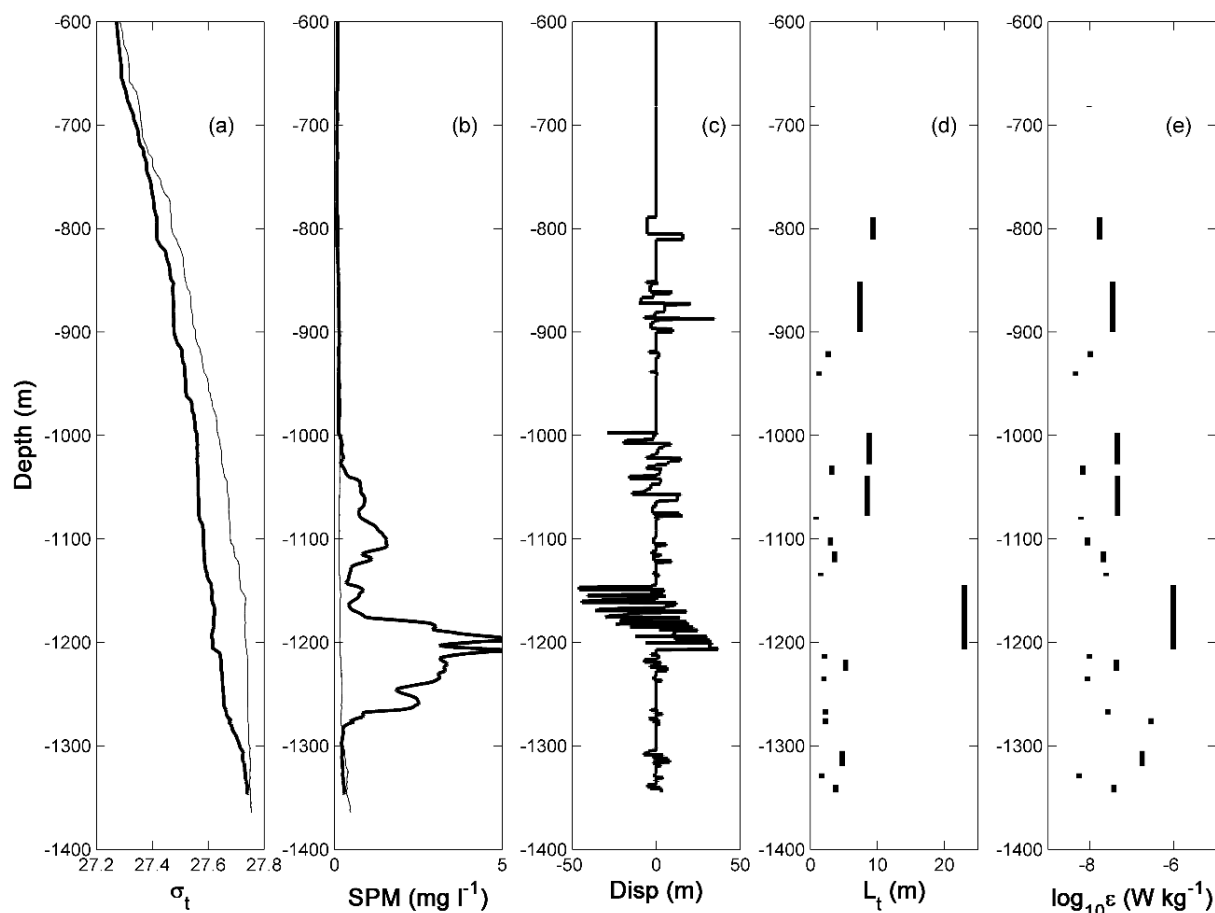


Fig. 9. Vertical profiles of (a)  $\sigma_t$ , (b) SPM (mg l<sup>-1</sup>), (c) Individual Thorpe displacements (m), (d) Thorpe Length Scale for overturns (m) and (e) log<sub>10</sub> of the turbulent energy dissipation ( $\epsilon$ , W kg<sup>-1</sup>), for the WC3 location at ~ 1385 water depth, 2013 (see Fig. 2a; K9). [Two columns wide]

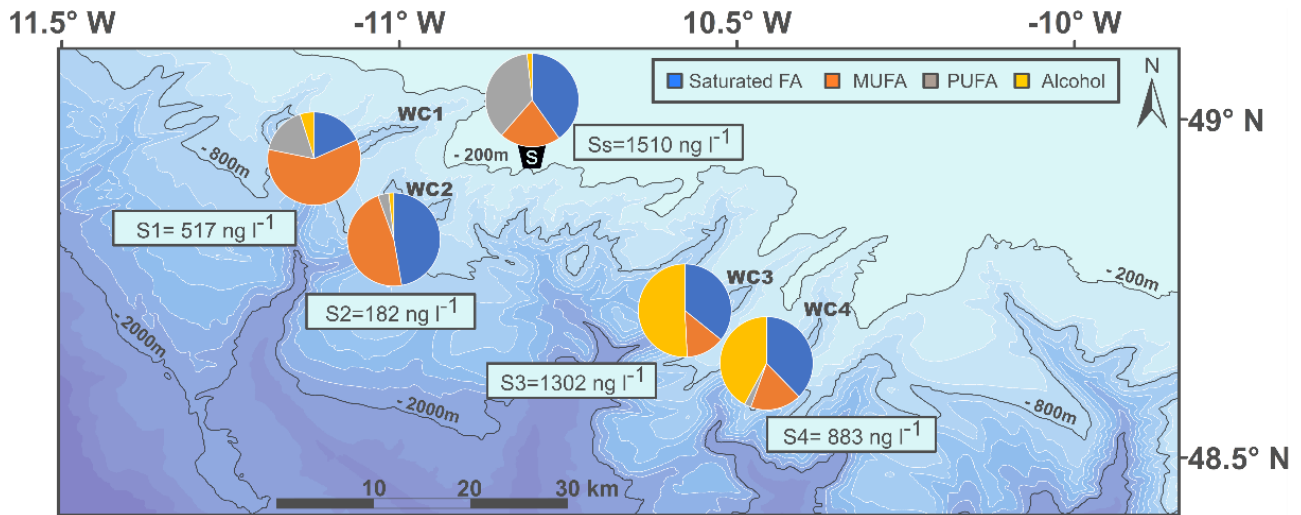


Fig. 10. Map image showing concentrations of total lipids normalised to volume of water ( $\text{ng l}^{-1}$ ) detected in suspended particulate organic matter collected in four branches (WC1 – 4) and at the surface of Whittard Canyon in June 2013. Pie charts show the contribution of saturated fatty acids, monounsaturated fatty acids (MUFAs), polyunsaturated fatty acids (PUFAs) and fatty alcohols in each sample (locations: S1 – 4 and surface sample Ss; see Fig. 2a). [1.5 columns wide]

591  
592  
593  
594  
595  
596  
597  
598  
599  
600  
601  
602  
603  
604  
605  
606  
607  
608  
609  
610  
611  
612  
613  
614  
615  
616  
617  
618  
619  
620  
621  
622  
623  
624  
625  
626  
627  
628  
629  
630  
631  
632  
633  
634  
635  
636  
637  
638  
639  
640  
641  
642  
643  
644  
645  
646  
647  
648  
649

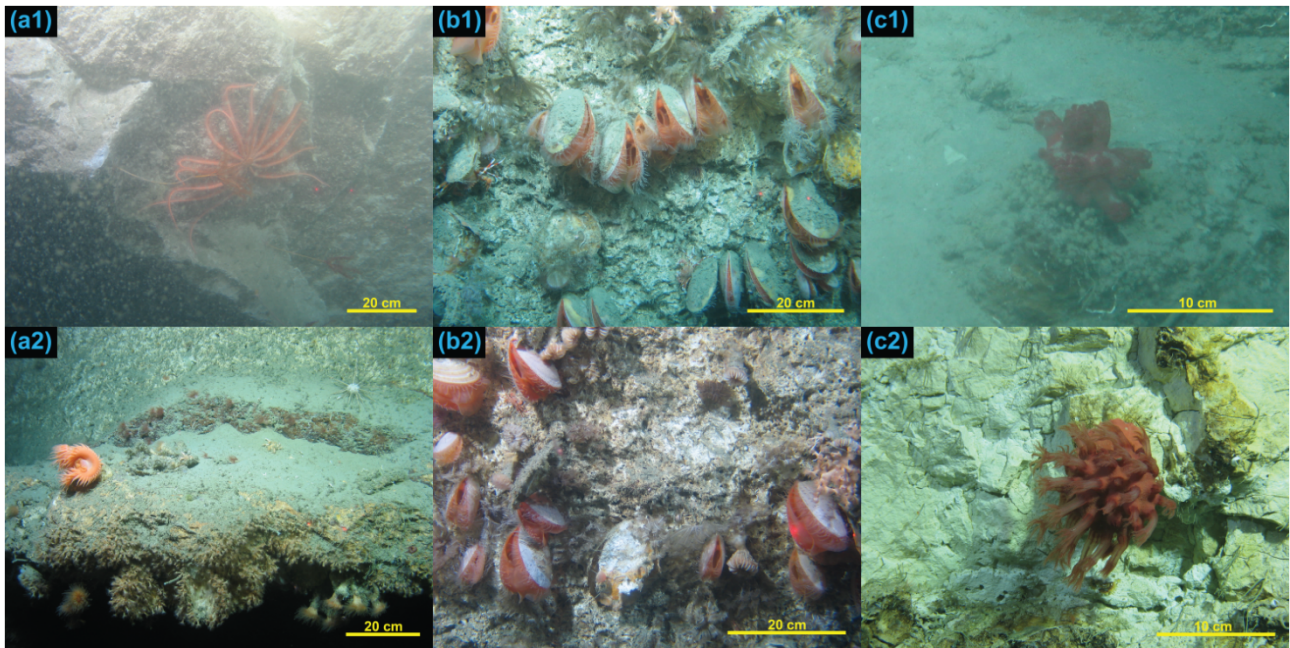


Fig. 11. Photo images from Whittard Canyon 2013 – 2016, displaying contrasting sediment concentrations both in the water column and resettling on benthic fauna. (a1): Cloudy water surrounds a Brisingid starfish; WC3. (a2): Very clear water and a Flytrap anemone; WC1. (b1): Sediment laden *Acesta excavata*; WC3. (b2): Clean *A. excavata*; WC3. (c1): The soft coral *Anthomastus* topped with a veil of sediment; WC3. (c2): An *Anthomastus* perched on a canyon wall with polyps fully extended. Note that the *Anthomastus* (c1) with retracted polyps may have become sediment covered during earlier ROV manoeuvres adjacent to site (visibility was not sufficient to determine this from the video), but the quantity of loose sediment available for such coverage may have been introduced by trawling. [Two columns wide]

650  
651  
652  
653  
654  
655  
656  
657 Table 1. Generalised Additive Model (GAM) fits to predict rugosity values in the full  
658 dataset, excluding cells with zero fishing (n = 6241 grid cells). Model predictors: R =  
659 Rugosity, Ln = longitude, Lt = Latitude, V = VMS fishing hours, S = slope angle.  
660 Variables in brackets have been modelled as interacting predictors. Generalised Cross  
661 Validation (GCV) scores indicate the relative performance of models, with lower values  
662 indicating better fits. Adjusted  $R^2$  values are a less robust indicator of model fit, but are  
663 included as their interpretation is more intuitive as an indicator of the performance of  
664 models at fitting the data.  
665  
666  
667  
668  
669  
670  
671  
672

673 <b>Model</b>	674 <b>Terms</b>	675 <b>GCV x10<sup>-5</sup></b>	676 <b>Adj R<sup>2</sup> %</b>
677 1	678 Ln + Lt	679 6.12	680 38.9
681 2	682 S + V	683 3.39	684 64.1
685 3	686 Ln + Lt + S + V	687 2.51	688 74.9
689 4	690 (Ln x Lt x S x V)	691 2.53	692 74.9
693 5	694 (Ln x Lt) + V	695 4.81	696 52.1
697 6	698 (Ln x Lt) + (S x V)	699 2.46	700 75.6
701 7	702 (Ln x Lt) + S	703 2.49	704 55.2

Table 2: Fishing intensity (hrs/km<sup>2</sup>) for each canyon branch, showing results for whole branches and also broken down into specific areas within branch.

	Whole canyon branch			Shallower and higher fished interfluves			Areas directly above 20° slope		
	Fishing	Area	Effort	Fishing	Area	Effort	Fishing	Area	Effort
	(hours)	(Km <sup>2</sup> )	(hrs/km <sup>2</sup> )	(hours)	(Km <sup>2</sup> )	(hrs/km <sup>2</sup> )	(hours)	(Km <sup>2</sup> )	(hrs/km <sup>2</sup> )
<b>WC1</b>	5755.6	220.4	26.1	5264.4	101.0	52.1	54.3	10.0	5.4
<b>WC2</b>	5926.7	264.8	22.4	5766.4	92.1	62.6	133.6	12.0	11.1
<b>WC3</b>	8847.2	214.1	41.3	8423.5	118.1	71.3	196.5	12.4	15.9
<b>WC4</b>	11132.3	260.9	42.7	10779.5	135.5	79.6	278.6	13.1	21.3

Table 3. Biogeochemical data for four samples (Locations S1 – 4; see Fig. 2a) and the surface sample (Ss) used in this study with mean  $\pm$  standard deviation for Western and Eastern samples. SPM: suspended particulate matter; C:N: molar carbon to nitrogen ratio; MUFA: monounsaturated fatty acids; PUFA: polyunsaturated fatty acids. Individual compounds, lipid group and primary biomarkers used for indices are shown in the Appendix. \* indicates torn filters

Variable	Unit	SURFACE	WEST				EAST			
Branch		*	WC1*	WC2*			WC3*	WC4		
Sample depth (mab)		12	1308 (12 mab)	1335 (20 mab)	mean	SD	1370 (7mab)	1368 (15mab)	mean	SD
SPM	mg l <sup>-1</sup>	NA	1.18	0.43	0.80	0.53	0.29	2.16	1.23	1.32
C/N	Molar	6.36	22.19	9.25	15.72	9.15	19.52	8.16	13.84	8.03
Total lipids normalised to water	ng l <sup>-1</sup>	1510.44	517.07	181.50	349.29	237.29	1301.85	882.74	1092.30	296.36
Saturated fatty acids	ng l <sup>-1</sup>	607.40	94.96	85.79	90.37	6.48	465.90	332.84	399.37	94.09
MUFA	ng l <sup>-1</sup>	319.84	309.20	85.66	197.43	158.07	174.37	157.16	165.77	12.17
PUFA	ng l <sup>-1</sup>	556.22	87.29	6.87	47.08	56.86		20.72	20.72	
Alcohol	ng l <sup>-1</sup>	26.98	25.63	3.18	14.40	15.87	661.58	372.03	516.80	204.75
Saturated fatty acids	%	40.21	18.36	47.27	32.82	20.44	35.79	37.70	36.75	1.36
MUFA	%	21.18	59.80	47.19	53.50	8.91	13.39	17.80	15.60	3.12
PUFA	%	36.82	16.88	3.79	10.33	9.26	0.00	2.35	1.17	1.66
Alcohol	%	1.79	4.96	1.75	3.35	2.26	50.82	42.14	46.48	6.13
Unsaturated fatty acids	%	58.00	76.68	50.98	63.83	18.17	13.39	20.15	16.77	4.78
<b>INDICES</b>										
Phyto	ng l <sup>-1</sup>	1182.73	315.85	136.39	226.12	126.90	1222.93	820.26	1021.59	284.73
	%	78.30	61.09	75.15	68.12	9.94	93.94	92.92	93.43	0.72
	ng l <sup>-1</sup>	66.85	25.92	13.93	19.93	8.47	20.50	29.83	25.17	6.60
Bacterial	%	4.43	5.01	7.68	6.35	1.88	1.57	3.38	2.48	1.28

## Appendix [supplementary data]

List of compounds most commonly identified in this study with groups and their corresponding IUPAC names. Individual compounds used for the phytoplankton and bacterial indices are indicated.

Compound	Group	IUPAC name	Reference for lipid biomarker/indices
br-C14:1	MUFA	Tetradecanoic acid (double bond position unknown)	
C14:1 (n-5)	MUFA	9-Tetradecenoic acid	
C14:0 acid	SFA	Tetradecanoic acid	<u>Phytoplankton</u> (Conte et al. 2003; Harwood and Russell, 1984)
C14:0 alcohol	Alcohol	Tetradecan-1-ol	<u>Phytoplankton</u> (Volkman et al., 1998)
C15:1(n-5)	MUFA	Methyl 10-cis-pentadecenoate	<u>Bacteria</u> (Volkman & Johns, 1977; Duineveld et al., 2012)
i-C15:0	BFA	12-Methyltetradecanoic acid	<u>Bacteria</u> (Volkman & Johns, 1977; Duineveld et al., 2012)
a-C15:0	BFA	12-Methyltetradecanoic acid	<u>Bacteria</u> (Volkman & Johns, 1977; Duineveld et al., 2012)
C15:0	SFA	Pentadecanoic acid	<u>Phytoplankton</u> (Conte et al. 2003; Harwood and Russell, 1984); <u>Bacteria</u> (Volkman & Johns, 1977; Duineveld et al., 2012)
br-C16:1	MUFA	Hexadecenoic acid (double bond position unknown)	
C16:1(n-7)	MUFA	9-Hexadecenoic acid	<u>Phytoplankton</u> (Conte et al. 2003; Harwood and Russell, 1984)
C16:0 acid	SFA	Hexadecanoic acid	<u>Phytoplankton</u> (Conte et al. 2003; Harwood and Russell, 1984)
C16:0 alcohol	Alcohol	1-Hexadecanol	<u>Phytoplankton</u> (Volkman et al., 1998)
br/st-C17:1	MUFA	Heptadecenoic acid double bond position unknown)	<u>Bacteria</u> (Volkman & Johns, 1977; Duineveld et al., 2012)
C17:0 acid	SFA	Heptadecanoic acid	<u>Phytoplankton</u> (Conte et al. 2003; Harwood and Russell, 1984); <u>Bacteria</u> (Volkman & Johns, 1977; Duineveld et al., 2012)
C18:3(n-6)	PUFA		<u>Phytoplankton</u> (Duineveld et al. 2012)

886	C18:2(n-6)	PUFA		<u>Phytoplankton</u> (Duineveld et al. 2012)
887	C18:1(n-9)	MUFA		
888				
889	C18:1(n-7)	6,9,12- Octadecatrienoic acid		<u>Bacteria</u> (Volkman & Johns, 1977; Duineveld et al., 2012)
890				
891				
892				
893				
894	C18:0 acid	9,12- Octadecadienoic acid		<u>Phytoplankton</u> (Conte et al. 2003; Harwood and Russell, 1984)
895				
896				
897	C18:0 alcohol	9-Octadecenoic acid		<u>Phytoplankton</u> (Volkman et al., 1998)
898				
899				
900	C20:5(n-3)	11-Octadecenoic acid		<u>Phytoplankton</u> (Duineveld et al. 2012)
901				
902	C20:3	Octadecanoic acid	Eicosadienoic acid (double bond position unknown)	<u>Phytoplankton</u> (Duineveld et al. 2012)
903				
904	C20:2	1-Octadecanol	Eicosadienoic acid (double bond position unknown)	<u>Phytoplankton</u> (Duineveld et al. 2012)
905				
906				
907	C20:1(n-9)	5,8,11,14,17- Eicosapentaenoic acid	11-Eicosenoic acid	
908				
909				
910	C20:0 acid	SFA	Eicosanoic acid	<u>Phytoplankton</u> (Conte et al. 2003; Harwood and Russell, 1984)
911				
912	C20:0 alcohol	Alcohol	1-Eicosanol	<u>Phytoplankton</u> (Volkman et al., 1998)
913				
914	C21:0 acid	SFA	Heneicosanoic acid	<u>Phytoplankton</u> (Conte et al. 2003; Harwood and Russell, 1984)
915				
916				
917	C22:6 (n-3)	PUFA	Docosahexaenoic acid	<u>Phytoplankton</u> (Duineveld et al. 2012)
918	C22:1(n-9)	MUFA	Tetracos-15-enoic acid	
919				
920	C22:0 acid	SFA	Docosanoic acid	<u>Phytoplankton</u> (Conte et al. 2003; Harwood and Russell, 1984)
921				
922	C24:1 (n-9)	MUFA	Nervonic	
923				
924				
925				
926				
927				
928				
929				
930				
931				
932				
933				
934				
935				
936				
937				
938				
939				
940				
941				
942				
943				
944				